Engineering Structures 210 (2020) 110339

Contents lists available at ScienceDirect

Engineering Structures

journal homepage: www.elsevier.com/locate/engstruct

Functionally graded graphene reinforced composite structures: A review

Shaoyu Zhao[a], Zhan Zhao[b], Zhicheng Yang[c], LiaoLiang Ke[d], Sritawat Kitipornchai[a], Jie Yang[b,*]

[a] School of Civil Engineering, The University of Queensland, St. Lucia, QLD 4072, Australia
[b] School of Engineering, RMIT University, PO Box 71, Bundoora, VIC 3083, Australia
[c] College of Urban and Rural Construction, Zhongkai University of Agriculture and Engineering, Guangzhou, China
[d] School of Mechanical Engineering, Tianjin University, Tianjin 300350, China

ARTICLE INFO

Keywords:
Functionally graded materials
Graphene platelets
Composite structures
Mechanical analysis
Micromechanics model

ABSTRACT

Owing to their superior mechanical properties, e.g. exceptionally high Young's modulus, high strength, large specific surface area, and good thermal conductivity, graphene and its derivatives such as graphene platelets (GPLs) are excellent reinforcing nanofillers for composite materials. The most recently developed functionally graded graphene platelets reinforced composite (FG-GPLRC) where GPLs are non-uniformly dispersed with more GPLs in the area where they are most needed to achieve significantly improved mechanical performance has opened up a new avenue for the development of next generation structural forms with an excellent combination of high stiffness, light weight and multi-functionality. Research activities in this emerging area have been rapidly increasing since it was first proposed in 2017. The present paper (i) briefly reviews the mechanical properties of graphene and graphene composites; (ii) summarizes the characteristics of functionally graded materials (FGM) and reports the fabrication of FG-GPLRC; (iii) discusses the existing micromechanics models for the prediction of effective mechanical properties of GPLRC; (iv) presents a comprehensive review on the mechanical analyses of FG-GPLRC structures; and (v) discuss the key technical challenges and future research directions.

1. Introduction

Carbonaceous nanomaterials with unique mechanical properties have shown tremendous potentials to be used as reinforcement fillers in developing advanced nanocomposites. Carbon nanotubes (CNTs) have attracted a lot of attention since it was discovered by Iijima in 1991 because of their very high mechanical strength (approximately 100 times greater than that of steel) and elastic modulus (around 1 TPa) as well as excellent electrical and thermal conductivities [1]. Large aspect ratio (1–10 nm in diameters and in the order of millimeters in length [2]) is another merit which makes it a promising candidate as reinforcement material for composites [3,4]. More recently, graphene which is a single-atom thick sheet of sp^2 hybridized carbon atoms with exceptionally high elastic modulus, tensile strength and very large specific surface area (about 3 times that of CNTs or even bigger) has inspired huge interests among research and industry communities since its discovery by Novoselov et al. in 2004 [5]. It has been reported in many experimental studies that graphene reinforced nanocomposites exhibit significant improvement in mechanical properties as compared to carbon nanotube composites [6].

Functionally graded materials (FGMs) are characterized by a continuous spatial gradient in both material composition and properties which are designable and can be tailored to meet the desired structural performance of the composite [7,8]. Since the novel multilayer functionally graded (FG) graphene platelets (GPLs) reinforced composites (FG-GPLRC) was first proposed by Yang and his coworkers [9–11], the mechanical behaviors of FG composites reinforced by GPLs or graphene sheets under various loading conditions have been an area of extensive research efforts worldwide. This is evidenced by a fast growing number of publications and citations in this research field over the past three years. As can be seen from Fig. 1a that is based on the data from Web of Science as of 8 January 2020, the total number of publications increases from 26 in 2017 to 140 in 2019 and the citations on the papers published in 2017 amounts to about 1700. The geographical distribution of the publications in Fig. 1b shows that the Asia and Pacific region is the home of the majority of the research activities in this area with more than 90% of the published works from this region.

This review article is organized as follows. Section 2 briefly introduces the mechanical features of graphene, graphene-based nanocomposites and FGMs. Section 3 reviews and compares micromechanics based models for the determination of effective material properties of grapehen or GPL reinforced composites. Section 4 present a comprehensive review on the state-of-the-art on the mechanical analyses of FG-GPLRC structures such as beams, arches, plates, shells subjected to

* Corresponding author.
E-mail address: j.yang@rmit.edu.au (J. Yang).

https://doi.org/10.1016/j.engstruct.2020.110339
Received 11 January 2020; Received in revised form 2 February 2020; Accepted 2 February 2020

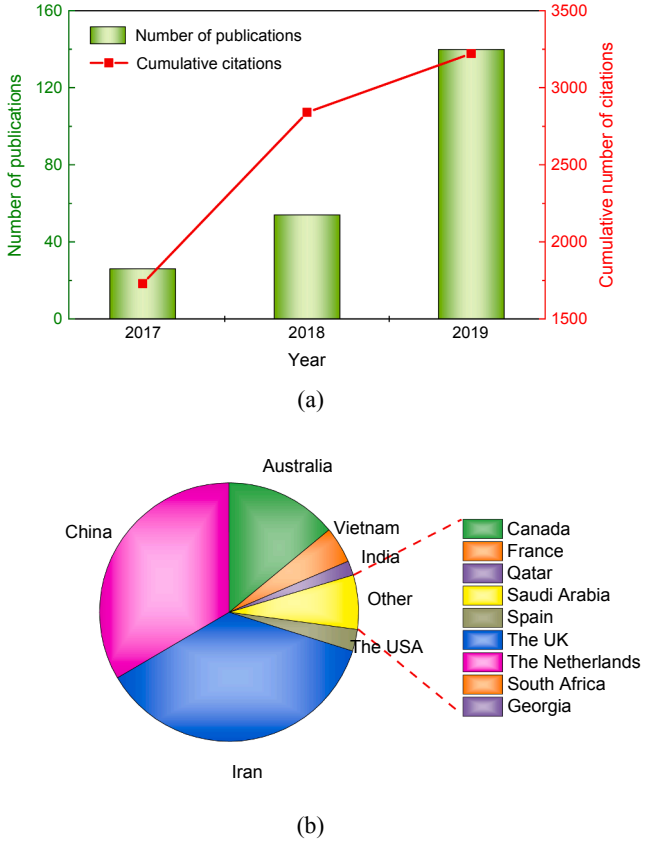

Fig. 1. (a) The total number of publications on functionally graded graphene reinforced structures and citations received; (b) geographical distribution of the research works in the research field by country (data from Web of Science, as of January 2020).

various loading conditions, followed by Section 5 in which key technical challenges and future research directions in this emerging area are discussed and identified.

2. Mechanical characteristics of graphene, graphene-based composites and FGMs

2.1. Mechanical properties of graphene

Graphene, a monolayer 2D honeycomb lattice structure composed of carbon atoms as shown in Fig. 2, is the basic structural element of all other graphitic carbon allotropes for different dimensionalities [12]. For instance, a graphene sheet can be wrapped up to form a zero-dimensional (0D) fullerene namely buckyball or rolled into a 1D cylinder of carbon allotropes, i.e. carbon nanotubes. Stacking different number of graphene sheets together, single layer graphene, few layer graphene, graphene platelets, or graphite (3D carbon allotrope) can be obtained [12,13].

Graphene possesses many fascinating physical and mechanical properties, such as exceptionally high Young's modulus, high strength, and excellent thermal conductivity [14]. Lee et al. [15] first measured the elastic properties and intrinsic strength of monolayer graphene using nano-indentation method in an atomic force microscope (AFM). They found that the Young's modulus of graphene is 1 ± 0.1 TPa and the intrinsic strength is 130 ± 10 GPa that are much higher than those of traditional metallic materials. These results are very close to the predicted values (Young's modulus $E = 1.05$ TPa and intrinsic strength is 121 GPa) based on density functional perturbation theory (DFPT) [16]. Table 1 summarizes the Young's modulus of graphene sheet experimentally measured or predicted through theoretical models that are available in open literature. It can be observed that the Young's modulus of graphene is about 1 TPa.

2.2. Mechanical properties of graphene-based composites

Due to its aforementioned exceptional mechanical properties, graphene has been widely used as the reinforcing nanofillers for polymer or metal based composites to achieve significantly improved mechanical performance. The performances of graphene reinforced composites depend strongly on nanofillers' dispersity. The most commonly used method to disperse graphene into polymer for synthesizing graphene-polymer composites include in situ polymerization processing, solution mixing processing and melt blending processing [23–27] while liquid metallurgy processing, powder metallurgy processing, electrochemical deposition processing, etc. [25,26,28–30] have been developed to disperse graphene into metal to fabricate graphene-metal composites.

Table 2 lists the percentage increase in both Young's modulus and tensile strength of polymeric and metallic nanocomposites with respect to their neat matrix counterparts due to the use of a very low concentration of graphene and its derivatives in terms of volume fraction (vol.%) or weight fraction (wt.%). xGnP, FG, GO, GPL, G, rGO, and GNS stand for exfoliated graphene nanoplatelets, functionalized graphene, graphene oxide, graphene nanoplatelets, graphene, reduced graphene oxide, and graphene nanosheets, respectively. Significant reinforcing effect can be observed from these experimental results. Since graphene and its derivatives are prone to agglomeration and poor dispersion, especially at a high concentration and this eventually lead to considerably deteriorated mechanical properties, only a low concentration (wt.% $< 1 \sim 3\%$) has been used in graphene nanocomposites.

2.3. Characteristics of FGMs

Functionally graded materials (FGMs) are non-homogenous composite materials in which the material composition and/or microstructure gradually change along one or more directions, leading to a continuous variation in mechanical, electrical and thermal properties of the material. The idea of functionally graded materials with compositional and structural gradients for polymeric materials was first proposed by Bever et al. [48,49] in 1972. The design and successful fabrication of functionally graded metal/ceramic thermal coating structure was reported by a group of Japanese scientists for hypersonic space plane in 1987 which has excellent resistance against high thermal flux and at the same time good capability of maintaining structural integrity and safety [50,51].

Compared with traditional composite structures, FGMs offer the following unique advantages: (i) the interfacial cracking or debonding caused by the stress concentration due to the abrupt change in material properties at the interface between two distinct materials that is very common in laminated composite structures can be effectively alleviated or eventually eliminated; (ii) the structure is multifunctional and can meet multiple different performance requirements simultaneously; and (iii) it can be used to develop advanced lightweight structures by making the best use of the material potentials.

The functionally graded structure reinforced with nanofillers can be formed through a gradient in the volume fraction, size, shape, or orientation of the nanofillers dispersed in the matrix, as shown in Fig. 3a-d [7]. Fig. 3e illustrates an ideal FGM in which the mixture of two distinct material phases changes continuously and smoothly from one side to another. Unfortunately, such an FGM is impossible to achieve due to the constraints of current manufacturing technology. As an alternative, a multilayer structure shown in Fig. 3f that consists of a number of layers in which the mixing ratio of constituent materials follows a layer-wise variation can be used as an excellent approximation of the ideal FGM structure when the total number of layers is sufficiently large.

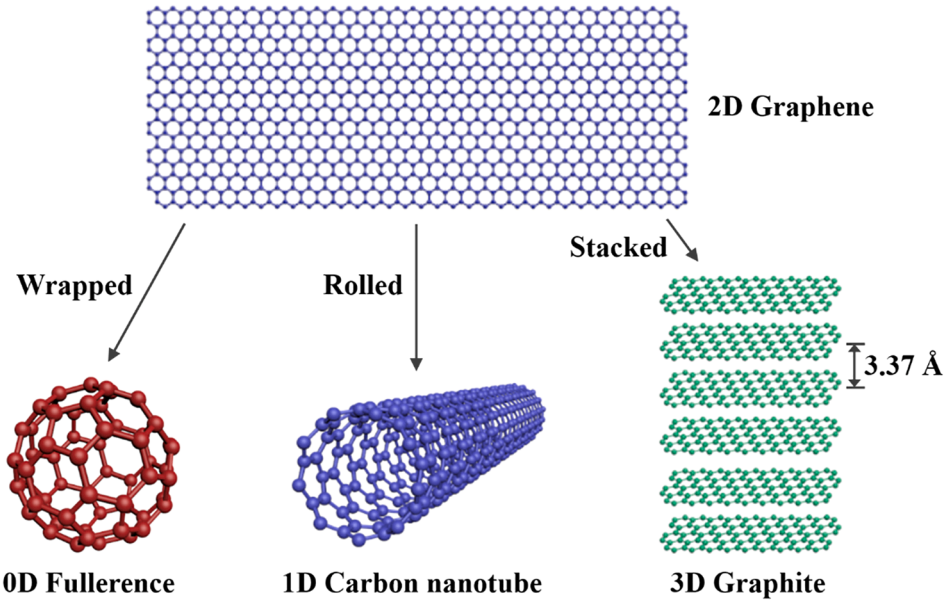

Fig. 2. From 2D graphene to 0D fullerene, 1D carbon nanotube and 3D graphite.

Table 1
Experimentally measured or theoretically predicted Young's modulus E of monolayer graphene.

Method	Thickness	E (TPa)	Publications
Experimental measurements			
Atomic Force Microscope	t = 0.335 nm	1 ± 0.1	Lee et al. [15]
Phonon Dispersion	t = 0.335 nm	1.020	Politano et al. [17]
Pressurized Blister Test	t = 0.335 nm	1.036	Koenig et al. [18]
Theoretical predications			
Ab Initio Study	t = 0.34 nm	1.110	Lier et al. [19]
Structural Mechanics based model	t = 0.34 nm	1.033	Li and Chou [20]
Density Functional Perturbation Theory	t = 0.334 nm	1.050	Liu et al. [16]
Continuum Mechanics	t = 0.34 nm	1.040	Shokrieh & Rafiee
Finite Element Method		1.140	[21]
Molecular Dynamics Simulation	t = 0.334 nm	1.150	Kvashnin and Sorokin [22]

2.4. Functionally graded graphene reinforced composites

Introducing the FGM concept into graphene based nanocomposites, Yang and his coworkers [9–11] proposed a novel class of multilayer functionally graded graphene platelets reinforced composites (FG-GPLRC) in which GPLs are randomly and uniformly distributed in each individual layer but its weight fraction changes in a layer-wise manner across the thickness direction. Their pioneering works on the static bending, free vibration and elastic buckling of FG-GPLRC beams indicate that their mechanical performances remarkably outperform their counterparts where GPLs are uniformly dispersed in the matrix. They have also developed a two-step approach as illustrated in Fig. 4a for the fabrication of FG-GPLRC which starts with the preparation of GPL nanofillers and epoxy matrix compound then mixing GPLs and epoxy through an appropriate dispersing and blending process. The well-mixed nanocomposite liquid is cast into a mold to obtain the first layer with a pre-designed GPL weight fraction. The above process is repeated to obtain the second single layer with a different GPL weight fraction. These two layers are bonded together through hot pressing before they are fully cured. Following this process to obtain and bond more single layers together sequentially, the multilayer FG-GPLRC can be fabricated. Fig. 4b shows the 6-layer FG-GPLRC sample that has been successfully fabricated through this two-step process and its tensile specimen prepared according to ASTM standards.

3. Micromechanics based models of effective material properties

Several micromechanics based models that take into account the effects of physical properties and/or geometric parameters of individual phase components have been developed and widely employed for the prediction of effective macroscopic mechanical properties of heterogeneous composite materials. These models include the rule of mixture (ROM) [52,53], shear-lag theory [54], Halpin-Tsai model [55,56], Eshelby's theory [57], Mori-Tanaka model [58], self-consistent model [59], Hashin-Shtrikman's theory [60,61], thermo-elastic model [62–64], effective medium theory model [65,66], etc.

3.1. Rule of mixture (ROM)

The ROM is the simplest model to predict the elastic properties of composite materials reinforced with unidirectional continuous fillers. According to Voigt's assumption of isostrain, the longitudinal modulus E_{11} can be obtained as

$$E_{11} = E_f V_f + E_m V_m \tag{1}$$

where E_f (E_m) and V_f (V_m) are the modulus and volume fractions of the filler (matrix), respectively.

To calculate the transverse elastic modulus of the composite, the transverse stress is considered to be equal in both the filler and the matrix according to Reuss's assumption. Accordingly, the transverse modulus E_{22} can be determined by the inverse rule of mixture (IROM),

$$\frac{1}{E_{22}} = \frac{V_f}{E_f} + \frac{V_m}{E_m} \tag{2}$$

For all nanofiller reinforced composites, the Young's modulus will be between the values predicted by the ROM and the IROM equation [67]. In another words, the Voigt model and Reuss model give the upper and lower bounds of the Young's modulus of the composites, respectively.

The in-plane shear modulus G_{12} can be derived using the similar method, i.e., based on equal shear stress assumption, as

$$\frac{1}{G_{12}} = \frac{V_f}{G_f} + \frac{V_m}{G_m} \tag{3}$$

Table 2
Percentage increase in Young's modulus and tensile strength of graphene based composites.

Matrix	Nanofiller	Concentration	Fabrication Process	% increase		Publications
				Young'sModulus	Tensile Strength	
Polymer matrix						
PP	xGnP-1	1 vol%	Melt	21	~	Kalaitzidou et al. [31,32]
		2 vol%		33	~	
		3 vol%		40	~	
PMMA	FG	1 wt%	Solution	80	~	Ramanathan et al. [33]
PVA	GO	0.7 wt%	Solution	62	76	Liang et al. [34]
Epoxy	GPL	0.1 wt%	Solution	31	40	Rafiee et al. [35]
PP	G	0.42 vol%	Melt	74	75	Song et al. [36]
Epoxy	FG	0.1 wt%	Melt	18	22	Naebe et al. [37]
Epoxy	GO	0.3 wt%	Solution	72	66	Pathak et al. [38]
PVA	GO	0.5 wt%	Solution	25	44	Wang et al. [39]
	rGO	0.3 wt%		32	48	
Metal Matrix						
Al	GNS	0.3 wt%	Powder	~	62	Wang et al. [40]
Cu	rGO	2.5 vol%	Mixing	30	30	Hwang et al. [41]
Al	rGO	0.75 vol%	Powder	8	29	Li et al. [42]
		1.5 vol%		21	50	
Al	G	1 wt%	Melt	36	15	Yolshina et al. [43]
		2 wt%		45	16	
Cu	GNP	0.5 vol%	Powder	~	49	Zhang and Zhan [44]
Ni				~	65	
Cu	Gr	1.6 vol%	In situ	18	40	Cao et al. [45]
		2.5 vol%		25	73	
Ni	G	3 wt%	In situ	~	310	Jiang et al. [46]
AZ91	GNS	0.1 wt%	Powder	~	28	Yuan et al. [47]
		0.3 wt%		~	48	
		0.5 wt%		~	56	

where G_f and G_m are the shear moduli of the filler and the matrix, respectively.

It is noted that E_{11}, E_{22}, and G_{12} are elastic and shear moduli of the composites reinforced with aligned continuous fillers. For composites with randomly oriented fillers, its Young's modulus E_c and shear modulus G_c can be calculated by [52],

$$E_c \cong \frac{3}{8}E_{11} + \frac{5}{8}E_{22} \tag{4}$$

$$G_c \cong \frac{1}{8}E_{11} + \frac{1}{4}E_{22} \tag{5}$$

The ROM model can also be used to predict the Poisson's ratio ν_c, mass density ρ_c and thermal expansion coefficient α_c,

$$\nu_c = \nu_f V_f + \nu_m V_m \tag{6}$$

$$\rho_c = \rho_f V_f + \rho_m V_m \tag{7}$$

$$\alpha_c = \alpha_f V_f + \alpha_m V_m \tag{8}$$

in which ν_f, ρ_f, and α_f (ν_m, ρ_m, and α_m) are Poisson's ratio, mass density, and thermal expansion coefficient of fillers (matrixes), respectively.

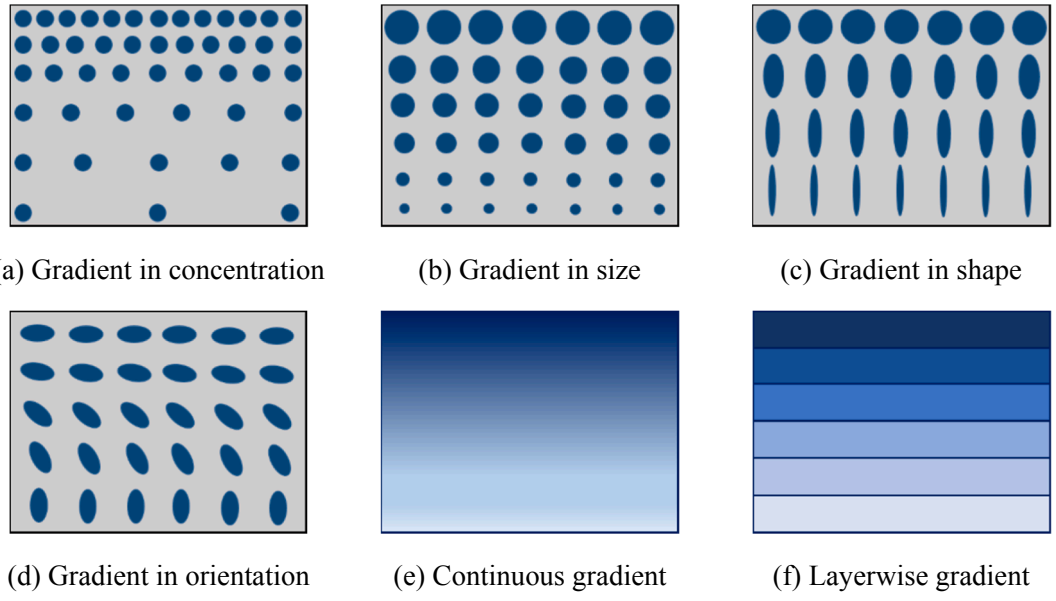

Fig. 3. Different types of FGM structures.

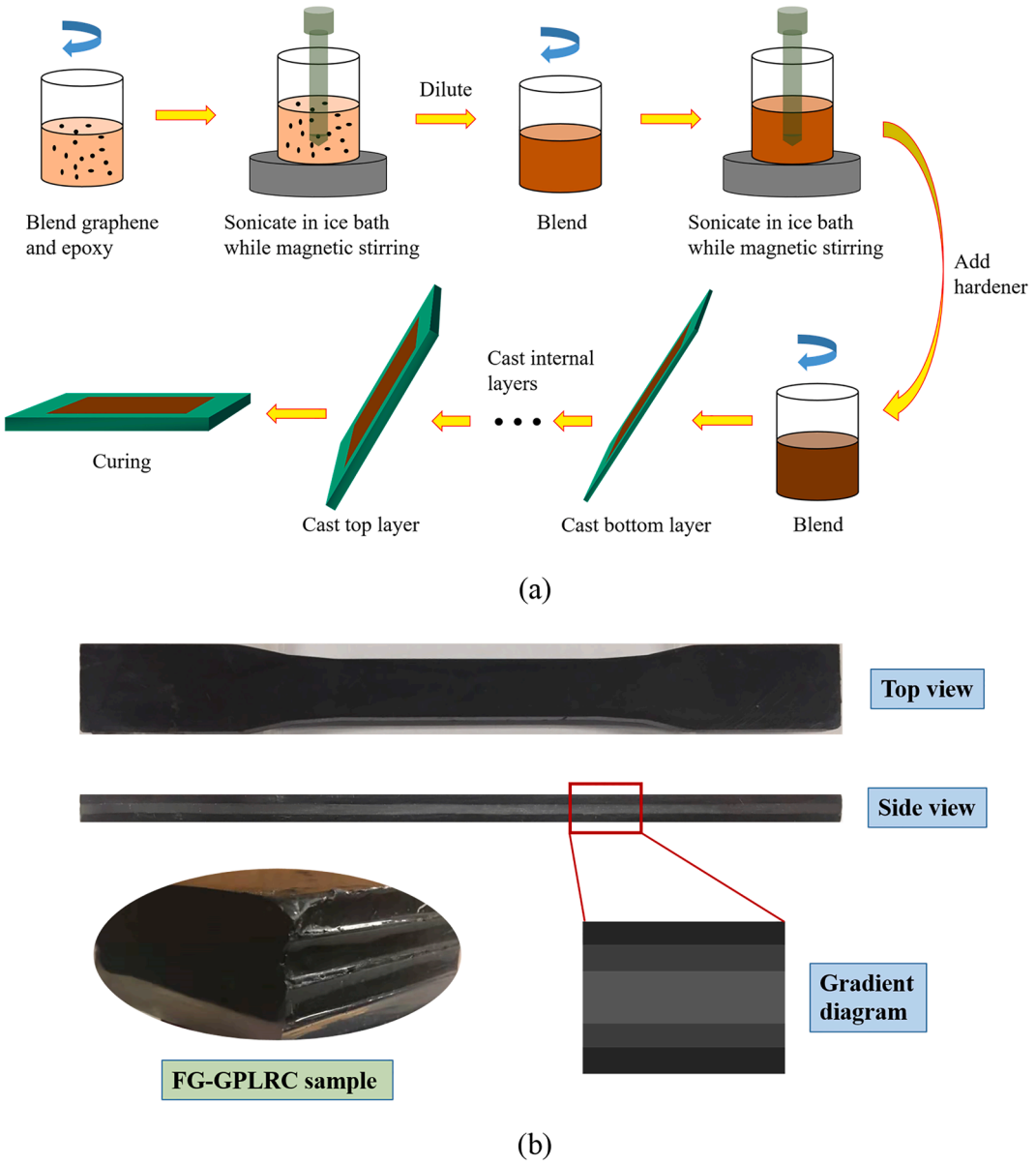

Fig. 4. (a) Two-step fabrication process of FG-GPLRC; and (b) a 6-layer FG-GPLRC sample and 6-layer ASTM tensile specimen.

3.2. Modified rule of mixture

As mentioned in previous section, elastic modulus E_{11} is deduced by ROM without considering the orientation and size of the filler. Therefore, a modified rule of mixture (MROM) has been proposed to predict the Young's modulus of composites reinforced by randomly distributed short discontinuous fillers.

$$E_c = \eta_0 \eta_1 E_f V_f + E_m V_m \tag{9}$$

where η_0 denotes the filler orientation distribution factor; and η_1 is the filler length distribution factor.

The filler orientation distribution factor η_0 can be expressed as [68],

$$\eta_0 = \cos^4(\alpha_0) \tag{10}$$

where α_0 is the filler orientation limit angle. The factor is equal to 1 for oriented fillers and 1/5 for randomly aligned fillers. Hence, the random orientation of the filler would lead to a reduced modulus.

Cox [54] derived the filler length distribution factor η_1 based on the shear-lag theory which is one of the most commonly used theory to predict the modulus of a randomly aligned discontinuous filler reinforced composite. This model is also named Cox model or shear-lag model. The length distribution factor η_1 for short filler can be obtained by,

$$\eta_1 = 1 - \frac{\tanh(\beta s)}{\beta s} \tag{11}$$

where s is the aspect ratio of fillers, and shear parameter β denotes the coefficient of stress concentration rate at the end of the fillers, which is given by

$$\beta = \sqrt{\frac{2E_m}{E_f(1+\nu_m)\ln(1/V_f)}} \tag{12}$$

where ν_m is the Poisson's ratio of the matrix. The length distribution factor η_1 takes values from 0 to 1, and is equal to 1 for a continuous filler.

3.3. Halpin-Tsai model

Halpin-Tsai model [55,56] is a semi-empirical method to predict the elastic properties of fibre reinforced composites. This model can take

into consideration the geometric characteristics and the orientation of the filler that would considerably affect the reinforcing efficiency. The longitudinal modulus E_{11}, the transverse modulus E_{22}, and the shear modulus G_{12} can be obtained as,

$$E_{11} = \frac{1 + \xi_{11}\eta_{11}V_f}{1 - \eta_{11}V_f}E_m \tag{13a}$$

$$E_{22} = \frac{1 + \xi_{22}\eta_{22}V_f}{1 - \eta_{22}V_f}E_m \tag{13b}$$

$$G_{12} = \frac{1}{1 - \eta_{12}V_f}G_m \tag{13c}$$

where η_{11}, η_{22} and η_{12} takes the following expression,

$$\eta_{11} = \frac{(E_f/E_m) - 1}{(E_f/E_m) + \xi_{11}} \tag{14a}$$

$$\eta_{22} = \frac{(E_f/E_m) - 1}{(E_f/E_m) + \xi_{22}} \tag{14b}$$

$$\eta_{12} = \frac{(G_f/G_m) - 1}{G_f/G_m} \tag{14c}$$

in which ξ_{11} and ξ_{22} are the shape size parameters along longitudinal and transverse directions. The reinforcement geometry factors have different expressions for different reinforcement shape. For platelets or lamellar-shaped fillers, ξ_{11} and ξ_{22} are defined as [9–11,56],

$$\xi_{11} = 2(l/t) \tag{15a}$$

$$\xi_{22} = 2(w/t) \tag{15b}$$

where l, w, and t represent the length, width and thickness of the rectangular filler, respectively. For cylindrical filler, thickness t should be changed to diameter d in Eq. (15), and $w = t = d$. Hence, $\xi_{11} = 2(l/d)$, $\xi_{22} = 2$ [56].

Submitting Eqs (13)–(15) into Eq. (4), the Young's modulus of the composite with randomly oriented reinforcement is given by,

$$E_c = \frac{3}{8}\frac{1 + \xi_{11}\eta_{11}V_f}{1 - \eta_{11}V_f}E_m + \frac{5}{8}\frac{1 + \xi_{22}\eta_{22}V_f}{1 - \eta_{22}V_f}E_m \tag{16}$$

3.3.1. Modified Halpin-Tsai model

It should be pointed out that all of the aforementioned existing models do not consider the effects of temperature [69,70], graphene defects [69,71,72], chemical functionalization of graphene fillers [72], etc., which play an important role in the reinforcement effectiveness of nanofillers. These models, therefore, should be modified to address this important issue. Based on extensive molecular dynamics simulation results, Sun et al. [69] introduced modification functions $f_{ii}(T)$ and $g_{ii}(\delta)$ $(i = 1, 2)$ to reflect the influences of the temperature and atom vacancy defects into the Halpin-Tsai model as

$$E_c = \frac{3}{8}\frac{1 + \xi_{11}\eta_{11}V_f}{1 - \eta_{11}V_f}f_{11}(T)g_{11}(\delta)E_m + \frac{5}{8}\frac{1 + \xi_{22}\eta_{22}V_f}{1 - \eta_{22}V_f}f_{22}(T)g_{22}(\delta)E_m \tag{17}$$

Their study indicated that the modified Halpin-Tsai model gives results in excellent agreement with MD simulation results while the original Halpin-Tsai model significantly overestimates the Young's modulus and this error tends to be much bigger as GPL weight fraction increases, in particular, when wt.% > 0.5%.

By introducing three graphene efficiency parameters into the Halpin-Tsai model and matching the elastic moduli of graphene reinforced composite obtained by MD simulation and the model, Shen et al. [73–77] proposed another modified version for Halpin-Tsai model as below,

$$E_{11} = \gamma_1\frac{1 + \xi_{11}\eta_{11}V_f}{1 - \eta_{11}V_f}E_m \tag{18a}$$

$$E_{22} = \gamma_2\frac{1 + \xi_{22}\eta_{22}V_f}{1 - \eta_{22}V_f}E_m \tag{18b}$$

$$G_{12} = \gamma_3\frac{1}{1 - \eta_{12}V_f}G_m \tag{18c}$$

where γ_j $(j = 1, 2, 3)$ are the graphene efficiency parameters.

It is worthy of noting that the modified model in Eq. (17) is for composites in which graphene sheets or GPLs are randomly oriented and uniformly dispersed hence the composite is macroscopically isotropic whereas Eq. (18) is for composites reinforced with aligned graphene sheets and considered to be anisotropic due to the slight anisotropy of the graphene sheet.

Rafiee et al. [35] also modified the Halpin-Tsai model (Equation 13) by changing the shape size parameters ξ_{11} and ξ_{22} to predict the Young's modulus of graphene reinforced nanocomposites according to their experimental results. The modified parameters are given as

$$\xi_{11} = 2\left(\frac{(w + l)/2}{t}\right) \tag{19a}$$

$$\xi_{22} = 2 \tag{19b}$$

3.4. Mori-Tanaka model

Mori-Tanaka model [58,78] is widely used for particle reinforced composites. The Young's modulus E_c and Poisson's ratio ν_c are evaluated through the following equations,

$$E_c = \frac{9K_cG_c}{3K_c + G_c} \tag{20a}$$

$$\nu_c = \frac{3K_c - 2G_c}{6K_c + 2G_c} \tag{20b}$$

where K_c and G_c are the bulk modulus and shear modulus of composites, which are given as,

$$K_c = K_m + \frac{V_f(K_f - K_m)}{1 + (1 - V_f)[3(K_f - K_m)/(3K_m + 4G_m)]} \tag{21a}$$

$$G_c = G_m + \frac{V_f(G_f - G_m)}{1 + (1 - V_f)[(G_f - G_m)/(G_f + f_m)]} \tag{21b}$$

in which

$$f_m = \frac{G_m(9K_m + 8G_m)}{6(K_m + 2G_m)} \tag{22a}$$

$$K_m = \frac{E_m}{3(1 - 2\nu_m)},\ K_f = \frac{E_f}{3(1 - 2\nu_f)},\ G_m = \frac{E_m}{2(1 + \nu_m)},\ G_f = \frac{E_f}{2(1 + \nu_f)} \tag{22b}$$

More detailed descriptions of this model can be found in Refs [58,78].

This model was modified by Tandon and Weng [79] by combining Eshelby's theory [57] and Mori-Tanaka's theory [58]. The longitudinal modulus E_{11} and transverse modulus E_{22} can then be expressed as,

$$E_{11} = \frac{1}{1 + V_f(A_1 + 2\nu_mA_2)/A}E_m \tag{23a}$$

$$E_{22} = \frac{1}{1 + V_f[-2\nu_mA_3 + (1 - \nu_m)A_4 + (1 + \nu_m)A_5A]/2A}E_m \tag{23b}$$

where the expressions of the parameters A and A_n are given in Ref. [79].

3.5. Thermoelastic model

(1) Thermal expansion coefficient

Thermal expansion coefficient is an important thermal property in the determination of the thermo-mechanical behavior of FG-GPLRC subjected to a temperature change. According to Schapery model [62], the longitudinal thermal expansion coefficient α_{11} and the transverse thermal expansion coefficient α_{22} of graphene reinforced composite are given by [73,74,80],

$$\alpha_{11} = \frac{\alpha_f V_f E_f + \alpha_m V_m E_m}{V_f E_f + V_m E_m} \tag{24a}$$

$$\alpha_{22} = (1 + \nu_f)\alpha_f V_f + (1 + \nu_m)\alpha_m V_m - \alpha_{11}\nu_c \tag{24b}$$

Other models that have been used to calculate the thermal expansion coefficient of the composite include ROM, Turner model [81], Kerner's model [82], Rosen and Hashin's theory [83], etc.

(2) Thermal conductivity

The thermal conductivity k_c of composites reinforced by randomly dispersed nanofillers can be obtained based on the micromechanics theory [63,64]. Yang et al. [84–86] used this thermal conductivity model to analyze the thermoelastic behaviors of FG-GPLRC plates.

$$\frac{k_c}{k_m} = 1 + \frac{V_f}{3}\left[\frac{2}{H + 1/(k_x/k_m - 1)} + \frac{1}{(1 - H)/2 + 1/(k_z/k_m - 1)}\right] \tag{25}$$

in which k_m is the thermal conductivity of the matrix, H indicates the geometrical factor depending on the aspect ratio ($s = l/t$), k_x and k_z are the thermal conductivities of the filler along in-plane and through-thickness directions, respectively, which are given below,

$$H = \frac{\ln[(s + \sqrt{s^2 - 1})s]}{\sqrt{(s^2 - 1)^3}} - \frac{1}{s^2 - 1} \tag{26a}$$

$$k_x = \frac{k_f}{2R_k k_f/l + 1},\ k_z = \frac{k_f}{2R_k k_f/t + 1} \tag{26b}$$

where k_f represents the intrinsic thermal conductivity of the filler along in-plane direction and R_k is an average interfacial thermal resistance between the fillers and matrix.

3.6. Effective medium theory

In comparison with the micromechanics models reviewed above, the effective medium theory is capable of predicting both elastic and dielectric properties [65,66]. Wang et al. [87–89] employed this model to predict the effective elastic modulus and dielectric permittivity of GPLRC dielectric beams.

(1) Effective elastic modulus

The effective Young's modulus of the composite can be derived by,

$$V_m \frac{E_m - E_c}{E_c + (1/3)(E_m - E_c)} + \frac{1}{3}V_f \sum_{k=1}^{3} \frac{E_f^{kk} - E_c}{E_c + S^{kk}(E_f^{kk} - E_c)} = 0 \tag{27}$$

where E_f^{kk} is the Young's modulus of fillers; the superscript kk indicates the directions, e.g. E_f^{11} and E_f^{22} are the in-plane Young's modulus and E_f^{33} is the out-plane Young's modulus of fillers; S^{kk} is the Eshelby's tensor which depends on the aspect ratio of nanofillers and can be expressed as the following form by treating reinforcing fillers as thin oblate spheroid shape [65,66],

$$S_{11} = S_{22} = \begin{cases} \frac{s}{2(1 - s^2)^{3/2}}[\arccos s - s(1 - s^2)^{1/2}], & s < 1 \\ \frac{s}{2(s^2 - 1)^{3/2}}[s(s^2 - 1)^{1/2} - \arccos s], & s > 1 \end{cases} \tag{28a}$$

$$S_{33} = 1 - 2S_{22} \tag{28b}$$

in which s is the aspect ratio of fillers.

(2) Effective dielectric permittivity

In addition, the effective dielectric permittivity can be obtained as,

$$V_m \frac{\overline{\sigma}_m - \overline{\sigma}_c}{\overline{\sigma}_c + (1/3)(\overline{\sigma}_m - \overline{\sigma}_c)} + \frac{1}{3}V_f \sum_{k=1}^{3} \frac{\overline{\sigma}_f^{kk} - \overline{\sigma}_c}{\overline{\sigma}_c + S^{kk}(\overline{\sigma}_f^{kk} - \overline{\sigma}_c)} = 0 \tag{29}$$

where $\bar{\sigma}$ denotes complex electrical conductivity that is comprised of two parts, i.e. real part and imaginary part,

$$\overline{\sigma} = \sigma + 2\pi f_{AC}\varepsilon j \tag{30}$$

in which the first term σ is the direct current (DC) conductivity and the second imaginary part is the alternating current (AC) conductivity with f_{AC} being AC frequency of the electric field and ε being the dielectric permittivity of materials.

3.7. Comparisons of micromechanics models

In order to illustrate the performance of these models, Table 3 compares the Young's modulus results of GPL/epoxy composite predicted by micromechanics models against the experimental data [35]. The material parameters used are [35]: $E_m = 2.85$ GPa, $\rho_m = 1.18$ g/cm^3, $\nu_m = 0.3$ for epoxy matrix and $E_{GPL} = 1.01$ TPa, $\rho_{GPL} = 1.06$ g/cm^3, $\nu_{GPL} = 0.186$ for GPLs with length $l = 2.5$ μm, width $w = 1.5$ μm, and thickness $t = 1.5$ nm; the GPL volume fraction at 0.1 wt% is 0.112 vol%.

Rafiee et al. [35] fabricated GPL reinforced epoxy nanocomposite and experimentally reported that its Young's modulus is 31% higher than that of the pristine epoxy. The theoretical prediction based on the Halpin-Tsai model modified by Rafiee et al. [35] is 3.23 GPa, which is 13.6% lower than the experimental result (3.74 GPa) while the Halpin-Tsai model modified by Yang et al. [9–11] gives much more accurate result that is only 2.4% higher than the experimental data. Hence, this model has been well accepted and extensively used to calculate the elastic modulus of GPLRC, as summarized in Table A1 in Appendix.

It should be mentioned that Mori-Tanaka model is for particle reinforced composites rather than cylindrical or plate-like fillers reinforced composites [78,90]. The effects of GPL geometry and size are not included in ROM and Mori-Tanaka model but are considered in Halpin-Tsai model. The geometry factor in the Halpin-Tsai model modified by Rafiee et al. [35] is taken as $\xi_{22} = 2$ for short circular fiber nanofillers [56] but this value is invalid for graphene platelets and should be calculated according to Eq. (15). The thermo-elastic model can be employed to predict the thermal expansion coefficient and

Table 3
Young's modulus (GPa) of GPL/epoxy composite (0.1 wt%) predicted by different micromechanics models.

Theoretical models	Theoretical	Experimental [35]	Error (%)
Modified Halpin-Tsai model (Rafiee) [35]	3.23	3.74 GPa	−13.6
Rule of mixture	3.28		−12.3
Modified rule of mixture	3.07		−17.9
Modified Halpin-Tsai model (Yang) [9–11]	3.83		2.4
Mori-Tanaka model	3.37		−9.9

Note: The results by rule of mixture, modified rule of mixture, modified Halpin-Tsai model (Yang) and Mori-Tanaka model are calculated using the material parameters given above.

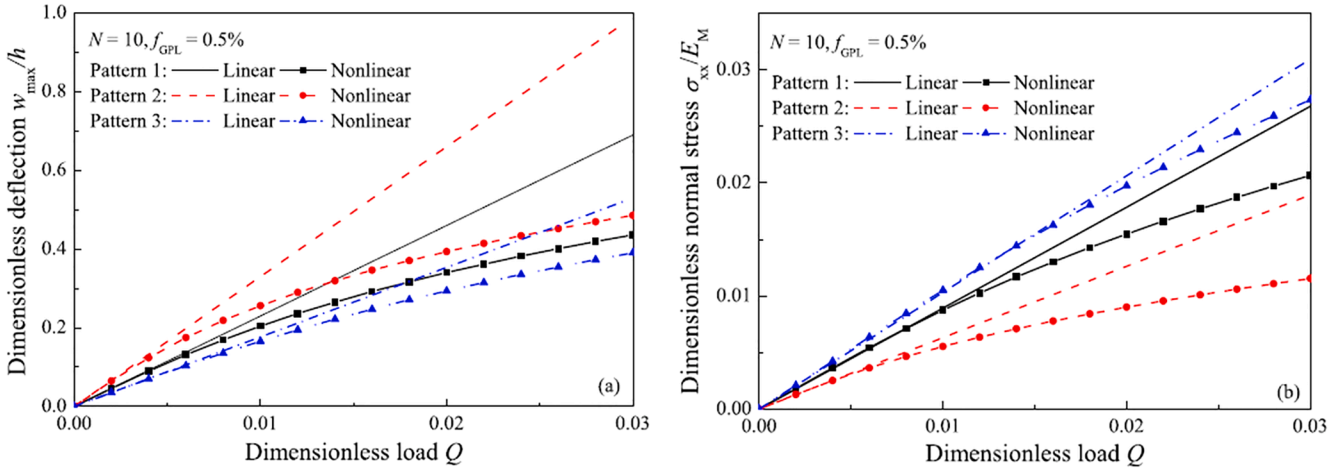

Fig. 5. Effect of GPL distribution pattern on nonlinear bending behaviors of H-H nanocomposite beams (a) Deflection; (b) Normal stres. [9].

thermal conductivity needed to study the mechanical behaviors of FG-GPLRC structures in thermal environments. The effective medium theory, however, can be used to determine the elastic properties together with the electrical attributes of GPL reinforced dielectric structures.

4. Mechanical analyses of FG-GPLRC structures

This section presents a comprehensive review on the analytical and numerical investigations on various mechanical behaviors of functionally graded graphene reinforced beams, arches, plates, and shells within the framework of three-dimensional elasticity theory or simplified one-dimensional (beams and arches) and two-dimensional (plates and shells) theories, with a particular focus on FG-GPLRC structures considering that the majority of the research works reported so far are concerned with this type of structures. The theoretical frameworks adopted in open literature are summarized in Table A2 in Appendix.

4.1. Linear bending analysis

4.1.1. Curved beams

Arefi et al. [91] presented a parametric study on the bending behavior of FG-GPLRC curved nanobeams by means of the first-order shear deformation theory (FSDT) and the nonlocal elasticity theory. Their results showed that the bending behaviors of curved beams are considerably affected by GPL weight fraction and its geometry. Polit et al. [92,93] studied the bending and stability behavior of the functionally graded porous (FGP) GPLRC curved beams based on a higher-order model considering thickness stretch effect and compared the deflection and stress solutions of the beam with those using other theories.

4.1.2. Plates

Based on the FSDT and by employing Navier's solution technique, Song et al. [94] presented the static bending analysis of multilayer FG-GPLRC plates. Li et al. [95] studied the static behavior of FGP plates reinforced with GPLs based on an isogemetric analysis within the framework of both FSDT and third-order shear deformation plate theories (TSDT). Furthermore, Zhao et al. [96] analyzed the static bending behaviors of FG-GPLRC trapezoidal plates by using the finite element method (FEM). Their results demonstrated that distributing more GPLs near the top and bottom surfaces of the plate is the most effective way in reinforcing the plate stiffness.

Different from the above mentioned investigations based on the Halpin-Tsai model [56], Garcia-Macias et al. [97] estimated the macroscopic elastic modulus of GPL reinforced composites by using the Mori-Tanaka model [58] and evaluated the load bearing capacity of GPLRC plates under static bending.

For FG-GPLRC structures under combined thermal-mechanical loading, Yang et al. [84–86] derived three-dimensional elasticity solutions for both bending deformation and stress distributions of FG-GPLRC rectangular plate, circular plate, annular plate and elliptical plate by employing the generalized Main-Spencer's method. The plates are subjected to a combined action of a uniformly distribution transverse load and a through-thickness steady temperature field. They found that dispersing GPL nanofillers according to FGX pattern, which does yield the smallest deflection, leads to very high bending stress as well. A modified FGX pattern that is capable of producing low deflection and stress results simultaneously was then suggested.

4.2. Nonlinear bending analysis

4.2.1. Beams

Feng et al. [9] first studied the nonlinear bending behavior of multilayer polymer composite beams with GPLs reinforcement based on Timoshenko beam theory and von Kármán geometric nonlinearity. It was found that the most effective way to improve the bending resistance is adding more GPLs near the top and bottom surfaces of the beam (Pattern 3), as shown in Fig. 5. Sahmani et al. [98] investigated nonlinear bending of porous micro/nano beams with graphene reinforcements by using nonlocal strain gradient theory. Rafiee et al. [99] developed a mathematical model to evaluate the effective material properties of GPLs/fiber/polymer multiscale composites and analyzed nonlinear behaviors of multiscale fiber-reinforced graphene composite beams. Shen et al. [73] investigated the large deflection behavior of graphene reinforced laminated beams and discussed the effects of temperature variation on the nonlinear bending of beams. The results shows that the GPLs reinforcement and the temperature changes have important impacts on the nonlinear bending behaviors of the beams.

For electro-mechanical performance of an FG-GPLRC beam with dielectric permittivity, Wang et al. [87] studied the dependency of its nonlinear bending behavior on the attributes of GPLs and the applied electrical field. Their results revealed that the AC frequency can dramatically change the structural behaviors of the beam, indicating the great potential of FG-GPLRC in smart structures and control.

4.2.2. Arches

In addition, nonlinear behaviors of FG-GPLRC porous arch structures were investigated by Liu et al. [100], which confirmed that the bending deformation of the arch is significantly reduced by using GPL reinforcements. The porosity distribution also plays an important role in its structural performance. Among the porosity distributions

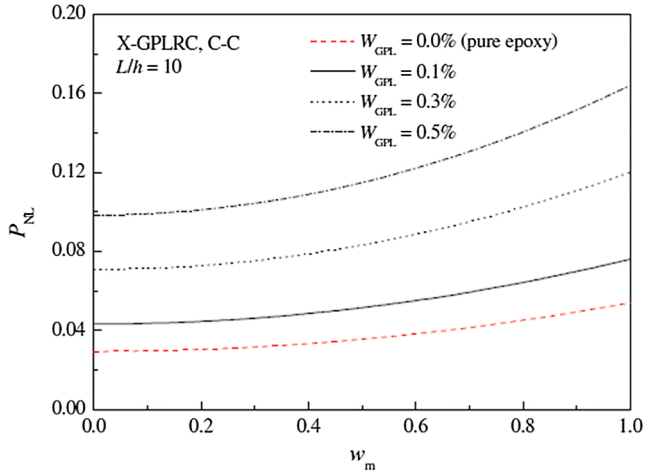

Fig. 6. Effects of GPL weight fraction on postbuckling paths of FG X-GPLRC beams [11].

considered in their study, the asymmetric porosity distribution gives the smallest deformation.

4.2.3. Plates

The geometrically nonlinear bending of FG-GPLRC trapezoidal plates was studied by Zhao et al. [101] based on the finite element method. Gholami and Ansari [102] studied the nonlinear bending of FG-GPLRC rectangular plates. Guo et al. [103] presented the nonlinear analysis of GPLRC quadrilateral plates using the element-free IMLS-Ritz method and concluded that the deflection of a quadrilateral plate is smaller than that of a square plate. By employing Reddy's third order shear deformation theory and a two-step perturbation method, Shen et al. [75,104] studied the nonlinear thermo-mechanical bending of functionally graded graphene reinforced laminated plates and cylindrical panels resting on an elastic foundation subjected to a temperature variation together with a transverse uniform or sinusoidal load.

4.3. Buckling analysis

4.3.1. Beams

Buckling performance is of crucial importance for structures under compression. Kitipornchai et al. [105] reported the buckling behavior of FGP beams reinforced by GPLs. Their results indicate that the critical buckling load of the porous beam can be effectively improved when both GPL dispersion and porosity distribution pattern are non-uniform and symmetric. Jiao and Alavi [106] discussed the buckling of graphene-reinforced metamaterial beams with periodic webbing patterns.

Tam et al. [107] and Song et al. [108] further studied the effect of open edge cracks on the buckling characteristics of FG-GPLRC beams by using FEM and an FSDT based analytical approach, respectively. Their results showed that the critical buckling load of FG-GPLRC beams is considerably affected by the crack. In the work by Song et al. [108], a massless rotational spring was used to model the bending stiffness of the cracked section that is related to the stress intensity factor at the crack tip.

4.3.2. Plates

Yang et al. [109] determined the uniaxial, biaxial and shear buckling loads of FG-GPLRC plates using Chebyshev-Ritz method and found that the non-uniformly symmetric porosity distribution and GPL pattern can achieve the best buckling resistance. Li et al. [95] investigated the static buckling of FG-GPLRC porous plates based on an isogeometric analysis. Other works on this topic include the thermal buckling analysis by Mirzaei and Kiani [110] who discussed the temperature dependent buckling behavior of FG-GPL reinforced laminated plates using a non-uniform rational B-spline (NURBS) based isogeometric finite element method and the one by Lei et al. [111] who carried out a parametric study on buckling behavior of FG-GPLRC laminated plates in thermal environment based on the FSDT and the meshless kp-Ritz method.

4.3.3. Shells

For FG-GPLRC shell structures, Wang et al. [112–114] investigated the eigenvalue buckling and torsional buckling of cylindrical shells with and without cutouts. It was concluded that square shaped GPLs with fewer single graphene layers are preferred reinforcements for better buckling resistance. Based on the three-dimensional elasticity theory, Liu et al. [115] obtained the three-dimensional buckling solutions of initially stressed FG-GPLRC cylindrical shells. It was found that thin shells with FGX dispersion pattern have a larger critical buckling load while for a thick FG-GPLRC shell the uniform GPL distribution pattern works the best.

4.4. Postbuckling analysis

4.4.1. Beams

Geometrically nonlinear strain-displacement relationship should be taken into consideration in postbuckling region. The first study on the postbuckling of FG-GPLRC beams is due to Yang et al. [11] who investigated the buckling and postbuckling behavior of such a beam using the FSDT and the differential quadrature method (DQM). Their results demonstrated that adding a small amount of GPLs significantly improved the buckling and postbuckling resistance of composite beams, as illustrated in Fig. 6. In addition, Barati and Zenkour [116] presented a postbuckling analysis of FG-GPLRC beams resting on a nonlinear hardening elastic foundation. The effects of porosity distribution and geometrical imperfections were discussed in detail. Other works dealing with the postbuckling performance of the beam include that by Rafiee et al. [99] who studied the nonlinear bending, thermal post-buckling and large amplitude vibration of multiscale fiber-reinforced graphene composite beams, and that by Kiani and Mirzzei [117] who investigated thermal buckling and postbuckling of temperature dependent GPL reinforced laminated beams based on the FSDT and von Kármán geometrical nonlinearity. The most recent notable work is by Song et al. [118] who conducted a comprehensive thermal buckling and postbuckling analysis on edge-cracked FG-GPLRC beams from which it was observed that the presence of an elastic foundation makes the buckling and postbuckling responses of FG-GPLRC beams much less sensitive to the crack. Wang et al. [88] studied the buckling and postbuckling of functionally graded dielectric composite beam with GPL reinforcements and found that the buckling performance of such a beam is remarkably influenced by the alternating current frequency within a certain range.

4.4.2. Arches

Yang et al. [119] analytically investigated the postbuckling behavior of FG-GPLRC arches either fixed or pinned at both ends within the framework of Euler-Bernoulli beam theory. Its nonlinear buckling behavior was found to be highly dependent on the GPL distribution. Huang et al. [120] did a similar work but both ends of the arch are constrained by elastic rotational supports. Yang et al. [121] further analyzed the thermo-mechanical postbuckling equilibrium paths of fixed FG-GPLRC shallow arches under a uniform radial pressure and a temperature change. Numerical results showed that the buckling performances of the arch can be greatly enhanced by distributing more GPLs near its surface layers.

4.4.3. Plates

For FG-GPLRC plate under edge compression, Song et al. [122] studied the buckling and postbuckling behaviors of biaxially compressed FG-GPLRC plates considering the effect of initial geometric imperfection based on the FSDT. Yang et al. [123] analyzed the

unilateral and bilateral buckling of FG-GPLRC corrugated thin plates and obtained the analytical solutions for the unilateral critical buckling load when the plate is resting on a rigid foundation and the bilateral critical buckling load when the plate is free from an elastic foundation. Wu et al. [124] examined the thermal buckling and postbuckling of FG-GPLRC plates within the framework of FSDT. Shen et al. [125–127] also investigated the postbuckling behaviors of functionally graded graphene reinforced sandwich plates, laminated plates and laminated cylindrical panels under axial compression or external pressure in thermal environments. In addition, Kiani [128] analyzed thermal buckling and postbuckling behaviors of FG-GPLRC plates by means of the TSDT.

4.4.4. Shells

The buckling and postbuckling of FG-GPLRC rings [129] and shells [90,130–134] have also been studied by several researchers. Dong et al. [130] analyzed the buckling behaviors of FG-GPLRC porous cylindrical shells with spinning motion under a combined action of external axial compressive force and radial pressure based on the FSDT. It was concluded that the buckling loads of the shell can be increased due to the centrifugal force caused by the spinning motion.

By employing the higher-order shear deformation shell theory (HSDT) and the von Kármán geometrical nonlinearity, Shen et al. [80,135] investigated postbuckling behaviors of temperature dependent GPL reinforced laminated cylindrical shells under axial compressive loads and external pressure and found that a piecewise graded distribution of graphene sheets can considerably enhance the critical buckling load/pressure and the postbuckling strength.

4.5. Linear free vibration analysis

4.5.1. Beams

The free vibration frequencies and the associated mode shapes are important characteristics for FG-GPLRC structures in engineering applications. Song et al. [108] investigated the linear flexural free vibration of edge-cracked shear deformable FG-GPLRC beams resting on an elastic foundation with the framework of the FSDT and a rotational spring model. The finite element analysis using PLANE183 elements was reported by Tam et al. [107]. Their results indicated that a crack located near the mid-span of the beam leads to the biggest drop in natural frequencies. In their study on the influences of GPL and porosity distributions on the free vibration of multilayer FG-GPLRC porous beams, Kitipornchai et al. [105] again confirmed the significant reinforcing effect of GPL nanofillers on both structural stiffness and natural frequencies. It was concluded from their comprehensive numerical results that non-uniformly symmetric porosity and GPL distributions can achieve the best vibration performance.

4.5.2. Plates

Song et al. [10] made the first attempt to study the free and forced vibration behaviors of FG-GPLRC plates. FSDT was employed to account for the effect of transverse shear strain. Navier solutions of the natural frequencies were obtained for plates simply supported on all edges. The effects of various boundary conditions on natural frequencies of FG-GPLRC plates were discussed by Reddy et al. [136]. Thai et al. [137] used the NURBS formulation based on the four-variable refined plate theory while Guo et al. [138] employed the element-free IMLS-Ritz method instead to study the free vibration of FG-GPLRC rectangular and quadrilateral plates. In addition, Malekzadeh et al. [139] analyzed the free vibration performance of FG-GPLRC eccentric annular plates embedded in piezoelectric layers based on the FSDT and the transformed DQM. Using the two-variable sinusoidal shear deformation theory and the nonlocal elasticity theory, Arefi et al. [140] discussed the small scale effect on the natural frequencies of FG-GPLRC nanoplates on a two-parameter Pasternak foundation.

4.5.3. Shells

Niu et al. [141] reported the free vibration characteristic of rotating pretwisted FG-GPLRC cylindrical shell panels and discussed the effects of distribution pattern, weight fraction, and geometry of GPLs, pretwisted angle, presetting angle and rotating speed on the natural frequencies. Their results also showed that the natural frequencies of the pretwisted shell panel rises greatly due to the addition of GPLs.

Dong et al. [142] investigated the linear free vibration of FG-GPLRC porous cylindrical shells with spinning motion and conducted a detailed parametric study on the natural frequencies and critical spinning speed of the shell that were found to be heavily affected by GPL distribution pattern and initial hoop tension. Based on Love's thin shell theory and the modified couple stress theory, Wang et al. [143] studied the size-dependent vibration of FG-GPLRC circular cylindrical shells. Besides, Wang et al. [144] analyzed the vibration behavior of FG-GPLRC doubly-curved thick shallow shells based on the HSDT.

Considering the thermal effects, Moradi-Dastjerdi and Behdinan [145] considered the free vibration behavior of FG-GPLRC axisymmetric thick cylinders under internal pressure and thermal gradient loads. They found that the temperature and hoop stress distributions of the cylinders are significantly influenced by the graphene distribution.

4.6. Nonlinear free vibration analysis

4.6.1. Beams

Feng et al. [146] investigated the nonlinear free vibration of FG-GPLRC beams based Timoshenko beam theory and von Kármán geometrical nonlinearity. Their results indicated that the nonlinear natural frequencies can significantly increase by adding a very small amount of GPLs and the most effective way to enhance the structural stiffness and rise the linear and nonlinear natural frequencies is distributing more GPLs near the top and bottom surfaces of the beam (Fig. 7).

For a closed-cell metal foam beam reinforced with GPL nanofillers, Chen et al. [147] studied its nonlinear free vibration behavior with internal pores and GPLs either uniformly or non-uniformly distributed. Timoshenko beam theory and Ritz method together with a direct iterative algorithm were used to calculate its nonlinear free vibration natural frequencies of the beams with different boundary conditions. For a simply supported functionally graded graphene reinforced thick laminated beam resting on an elastic foundation under a temperature change, Shen et al. [77] employed HSDT and a two-step perturbation technique to discuss its nonlinear vibration characteristics. Considering the electrical effects, Wang et al. [89] analyzed the nonlinear free vibration of GPL reinforced dielectric beams and found that the electrical field plays an important role on the nonlinear free vibration characteristics.

4.6.2. Plates

Based on classic plate theory and von Kármán geometrical nonlinearity, Gao et al. [148] reported the nonlinear free vibration analysis of FG-GPLRC porous plates resting on an elastic foundation. The differential quadrature method was used to calculate the nonlinear natural frequencies. Taking the thermal effects into consideration, Shen et al. [74,149] dealt with the nonlinear free vibration of shear deformable functionally graded graphene sheet reinforced laminated plates/cylindrical panels within the framework of HSDT. A similar work was done by Kiani et al. [150] for thermally prestressed thick composite plates reinforced with graphene sheets using a non-uniform rational B-spline (NURBS) based isogeometric finite element method. Considering the piezoelectric effect, Mao and Zhang [151] investigated the linear and nonlinear free vibrations of functionally graded piezoelectric plates reinforced with GPL nanofillers subjected to an external voltage excitation.

4.6.3. Shells

Except for the beam and plate structures, Dong et al. [152]

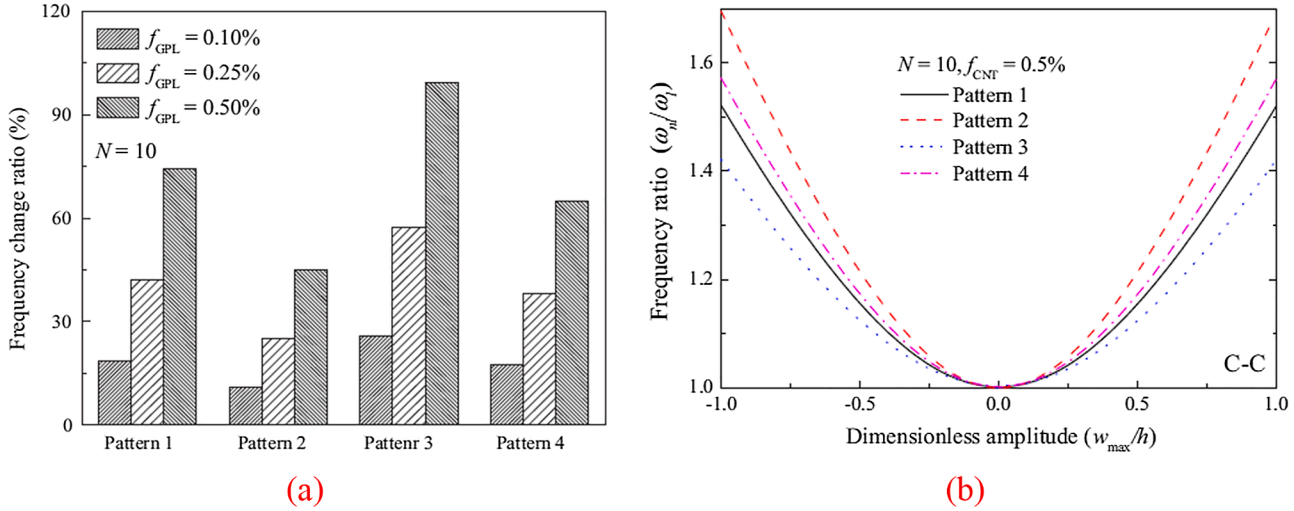

Fig. 7. (a) Effect of weight fraction of GPL on frequency change ratio of C-C beams; (b) Frequency ratio curves of C-C beams with different distribution patterns [146].

presented an analytical investigation on nonlinear free vibrations of spinning FG-GPLRC thin cylindrical shells based on the Donnell's nonlinear shell theory considering the effects of spinning motion and axial load. Wang et al. [153] conducted the nonlinear free vibration analysis of metal form cylindrical shells reinforced by GPLs. In addition, Shen et al. [154] carried out HSDT based nonlinear vibration analysis of functionally graded graphene sheet reinforced laminated cylindrical shells in thermal environments. Again, the two-step perturbation technique was used.

4.7. Dynamic instability analysis

A structural element may lose its stability when subjected to an axial periodic dynamic load that may contain a static force component. Wu et al. [155] identified the dynamic instability region of an FG-GPLRC beam by using Timoshenko beam theory and Bolotin's method. Their results, shown in Fig. 8, revealed that the dynamic stability of the beam can be greatly improved by adding a low content of GPL reinforcements.

Furthermore, Zhao et al. [156] analyzed the dynamic instability of FG-GPLRC porous arches pinned at both ends by means of classical Euler-Bernoulli beam theory. They concluded that the arch with GPL reinforcement and symmetrically non-uniform porosity distribution exhibits significantly enhanced dynamic stability. Yang et al. [157] also investigated the dynamic buckling of FG-GPLRC shallow arches under a step central point load. Apart from beam and arch structures, Wu et al. [158] reported the parametric instability characteristics of an FG-GPLRC plate under combined thermo-mechanical loading. Based on a two-step perturbation technique, Shen et al. [159] derived the equation of motion and determined the dynamic instability region for a simply supported functionally graded graphene reinforced plate.

4.8. Dynamic response analysis

4.8.1. Resonance response analysis

Li et al. [160] studied the primary, super-harmonic, subharmonic, and combinational resonances of FG-GPLRC beams by using the multiple scales method and found that an addition of a very low weight fraction of GPL nanofillers significantly reduces the resonant responses of the beams and the square shaped GPLs with fewer single graphene layers are the most favorable reinforcements, as illustrated in Fig. 9.

For plate structures, Karami et al. [161] investigated the forced resonance vibration behaviors of graphene reinforced nanoplates by using nonlocal strain gradient Kirchhoff plate theory. Gholami and Ansari [162] analyzed the nonlinear harmonically excited vibration of FG-GPLRC rectangular plates by means of the Galerkin method, time periodic discretization approach and pseudo arclength continuation

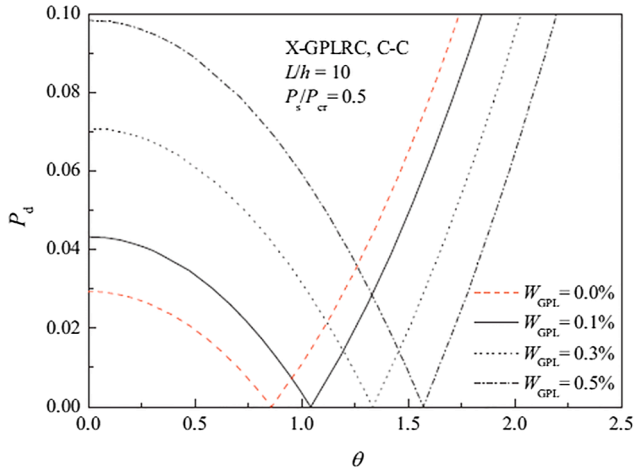

Fig. 8. Effect of GPL weight fraction on the principle unstable regions of FG X-GPLRC beams [155].

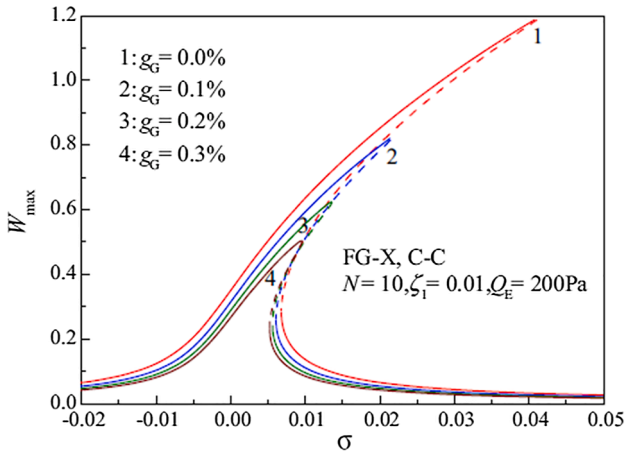

Fig. 9. Effect of GPL weight fraction on frequency-response for primary resonance [160].

technique with consideration of the modified Newton-Raphson method. Furthermore, Dong et al. [163] conducted the nonlinear harmonic resonance response analysis of spinning FG-GPLRC thin cylindrical shells subjected to a combined action of thermal loads and mechanical loads based on Donnell's nonlinear shell theory. They found that the resonance responses of the shell are significantly affected by the spinning motion.

4.8.2. Transient response analysis

Wang et al. [164] investigated transient responses of an FG-GPLRC beam subjected to two successive moving masses based on the HSDT. The results indicated that the dynamic response of the beam can be remarkably reduced through the addition of GPL nanofillers. Nguyen et al. [165] performed transient analysis of piezoelectric FG-GPLRC porous plates by employing an isogeometric Bezier finite element formulation. Li et al. [166] investigated nonlinear vibration of a composite plate consisting of two metal face layers and a functionally graded porous core with graphene platelet reinforcement based on the classical plate theory. They studied the effects of loading speed, temperature variation, initial imperfection, porosity parameters and GPL parameters on the transient response of the plate. In addition, Xu et al. [167] studied vibro-acoustic response characteristics of thermo-mechanically loaded FG-FPLRC laminated plate. Furthermore, Wang et al. [168] investigated the nonlinear transient dynamic response of FG-GPLRC doubly curved thick shallow shells subjected to blast loads within the framework of HSDT. It was observed from their study that the nonlinear transient response of the shell is considerably affected by the temperature field.

4.8.3. Impact response

The nonlinear dynamic responses of graphene reinforced beams [169], plates [170,171], and shells [172] under impact loads were conducted by several researchers. For example, Fan et al. [169] investigated the low-velocity impact response of FG-GPLRC beams in thermal environments. For FG-GPLRC plates, Song et al. [171] utilized the FSDT and modified nonlinear Hertz contact theory to define the contact force between the spherical impactor and the target plate and conducted a parametric study with a particular focus on the effects of GPL distribution pattern, weight fraction, geometry and size, temperature variation as well as the radius and initial velocity of the impactor on the low-velocity impact response of functionally graded GPLRC plates. It was found that dispersing more GPLs near the top and bottom surfaces can effectively resist the peak deflection in the process of impact but this will also give rise to a higher peak contact force. Moving the maximum GPL concentration away from the top and bottom layers to the midplane by a short distance is the most effective way to simultaneously reduce both peak deflection and contact force.

5. Challenges and future work

Functionally graded graphene reinforced composite structure with FG-GPLRC structure as its excellent representative has demonstrated great potentials for the development of new generation lightweight structures that are of crucial importance in aerospace, automotive, marine, mechanical, and other engineering sectors. Although many preliminary research works have been conducted in this emerging area, there are still many key technical challenges yet to be urgently addressed:

(1) Fabrication techniques of FG-GPLRC structures

As reported in many previous experimental studies, agglomeration and poor dispersion of graphene sheets and GPL nanofillers in polymeric or metallic matrix as well as the weak bonding at the interface between graphene and the matrix have been the major issues in the fabrication of graphene based nanocomposites as these problems will lead to poor or greatly deteriorated mechanical properties. New fabrication routes that can solve these problems should therefore be urgently developed. The manufacturing process for the mass production of FG-GPLRC and the technique for fabricating FG-GPLRC at micro-/nano-scale are also the great challenges ahead. Without the success in fabrication techniques, the real engineering applications of FG-GPLRC structures would be impossible.

(2) Micromechanics models

The micromechanics models summarized in Section 3, although having been widely used in the above reviewed open literature to determine the effective thermo-elastic properties of graphene reinforced composites, are simplified models based on various assumptions hence have their own limitations. For example, all of the existing models do not consider the influences of temperature [69,70], atom vacancy defects [69,71,72], functionalization of GPL nanofillers [72], uncertainty in GPL shape, size, and vacancy distribution, etc., which partly contribute to the significant discrepancy between the results obtained from experiments, MD simulation and these models, particularly, when GPL weight fraction wt.% > 0.5% [69].

In order to achieve more accurate and reliable numerical analysis results, more experiments and comprehensive MD simulation based parametric studies addressing the influence of the above mentioned factors should be carried out to obtain a sufficiently large set of data to modify the existing models.

(3) Mechanical analysis of FG-GPLRC structures

The majority of the mechanical and structural analyses of FG-GPLRC structures available in open literature are limited to elastic behaviors only, such as bending, buckling, postbuckling, free vibration, force vibration, impact response, dynamic stability of FG-GPLRC beams, plates and shells. For structural design in real engineering applications, an in-depth understanding of their inelastic deformation behavior, failure mechanism and failure criteria is essential. The research in this regard, however, is scarce. The only contributions are due to Song et al. [108,118] who most recently made the first attempt to study the stress intensity factor of an open edge crack perpendicular to the FG-GPLRC beam and discussed its influences on free vibration, thermo-mechanical buckling, and postbuckling performances of the beam. Up to now, no research work dealing with other crack defects (such as inclined crack, internal crack, breathing crack, etc.), crack initiation and propagation, microstructural damage, fracture, fatigue, etc. has been reported, in spite of their practical importance. Many fundamental questions are yet to be answered.

(4) Optimization design of FG-GPLRC structures

Furthermore, optimization of material profile, in particular, GPL distribution pattern towards optimal structural performance with balanced consideration of deformation and stresses is another important topic that requires special attention. Currently, most of the studies and the conclusions drawn from their numerical results are based on deformation analysis only but the stress analysis is not considered. This may lead to unsafe design since the GPL distribution that produces the smallest deformation will most likely results in the highest stress. A multi-objective optimization process is therefore necessary to identify the material profile and GPL distribution pattern that can achieve the desired structural performance targets.

6. Concluding remarks

Functionally graded composite structures reinforced with graphene sheets or GPLs have been proven to be very promising in a wide range of engineering applications where lightweight structures are of great

importance. In this paper, the state-of-the-art of FG-GPLRC structures since it was first proposed in 2017 has been comprehensively discussed and summarized. The review covers all of the important aspects in this emerging and fast growing area including the fabrication technique, micromechanics based models for the determination of effective material properties, atomistic studies via molecular dynamics simulation, analytical and numerical analyses of mechanical and structural behaviors of FG-GPLRC beam, plate, and shell structures under various loading conditions. The key technical challenges and future research directions have also been identified and highlighted.

Declaration of Competing Interest

The authors declare that they have no known competing financial interests or personal relationships that could have appeared to influence the work reported in this paper.

Acknowledgements

The work described in this paper was fully supported by the Australian Research Council grant under Discovery Project scheme (DP160101978), Australia. The authors are very grateful for these financial supports.

Appendix

(See Tables A1 and A2).

Table A1
Effective Young's modulus prediction models.

Micromechanical models	Publications
Modified Halpin-Tsai model (Yang)	[9–11,84–86,90–96,98–103,105,107–109,112–116,118–124,129–134,136–144,146–148,151–153,155–158,160–168,171–177]
Extended Halpin-Tsai model (Shen)	[73–75,77,80,104,110,111,117,125–128,135,149,150,154,159,169,170,178,179]
Mori-Tanaka model	[90,97]
Effective medium theory	[87–89]

Table A2
Theoretical frameworks.

Structures	Theories	Publications
Beam	Euler-Bernoulli beam theory	[99,156]
	First-order shear deformation beam theory (Timoshenko beam theory)	[9,11,87–89,91,105,108,117,118,146,147,155]
	Third-order shear deformation beam theory	[73,77,98,160,164,169,175]
	Trigonometric shear deformation beam theory	[92,93,177]
	Refined shear deformation beam theory	[116,174]
Plate	Classical plate theory (Kirchhoff theory)	[123,148,161,166]
	First-order shear deformation plate theory	[10,94,95,97,103,109–111,122,124,136,138,139,141,151,158,171,180]
	Third-order shear deformation plate theory	[74,75,95,125,126,128,150,159,162,165,167,170,179]
	Refined shear deformation plate theory	[137]
	Sinusoidal shear deformation plate theory	[102,140]
	Exponential shear deformation plate theory	[176]
Shell	Donnell's shallow shell theory (Thin-walled shell theory)	[100,119–121,129,157,173]
	Donnell's shell theory	[90,130–132,142,152,153,163,172,178]
	Love's thin shell theory	[143]
	First-order shear deformation shell theory	[90,130,142,178,181]
	Third-order shear deformation shell theory	[80,90,104,127,131,135,144,149,154,168]
	Refined hyperbolic shear deformation shell theory	[133,134]
3-D structures	Three-dimensional elasticity theory	[84–86,115]
Micro/nano-structures	Nonlocal elasticity theory	[91,140]
	Nonlocal strain gradient elasticity theory	[98,133,134,161,174–176]
	Modified couple stress theory	[106,143]

References

[1] Iijima S. Helical microtubules of graphitic carbon. Nature 1991;354:56–8.
[2] Iijima S, Ichihashi T. Single-shell carbon nanotubes of 1-nm diameter. Nature 1993;363:603–5.
[3] Lau AKT, Hui D. The revolutionary creation of new advanced materials—carbon nanotube composites. Compos B Eng 2002;33:263–77.
[4] Coleman JN, Khan U, Blau WJ, Gun'ko YK. Small but strong: A review of the mechanical properties of carbon nanotube–polymer composites. Carbon 2006;44:1624–52.
[5] Novoselov KS, Geim AK, Morozov SV, Jiang D, Zhang Y, Dubonos SV, et al. Electric field effect in atomically thin carbon films. Science 2004;306:666–9.
[6] Stankovich S, Dikin DA, Dommett GH, Kohlhaas KM, Zimney EJ, Stach EA, et al. Graphene-based composite materials. Nature 2006;442:282–6.
[7] Miyamoto Y, Kaysser WA, Rabin BH, Kawasaki A. Functionally graded materials: design, processing and applications. New York: Springer Science Business Media; 1999.
[8] Naebe M, Shirvanimoghaddam K. Functionally graded materials: A review of fabrication and properties. Appl Mater Today 2016;5:223–45.
[9] Feng C, Kitipornchai S, Yang J. Nonlinear bending of polymer nanocomposite beams reinforced with non-uniformly distributed graphene platelets (GPLs). Compos B Eng 2017;110:132–40.
[10] Song M, Kitipornchai S, Yang J. Free and forced vibrations of functionally graded polymer composite plates reinforced with graphene nanoplatelets. Compos Struct 2017;159:579–88.
[11] Yang J, Wu H, Kitipornchai S. Buckling and postbuckling of functionally graded multilayer graphene platelet-reinforced composite beams. Compos Struct 2017;161:111–8.
[12] Geim AK, Novoselov KS. The rise of graphene. Nat Mater 2007;6:183–91.
[13] Neto AC, Guinea F, Peres NM. Drawing conclusions from graphene. Phys World 2006;19:33–7.

[14] Akinwande D, Brennan CJ, Bunch JS, Egberts P, Felts JR, Gao H, et al. A review on mechanics and mechanical properties of 2D materials—Graphene and beyond. Extreme Mech Lett 2017;13:42–77.
[15] Lee C, Wei X, Kysar JW, Hone J. Measurement of the elastic properties and intrinsic strength of monolayer graphene. Science 2008;321:385–8.
[16] Liu F, Ming P, Li J. Ab initiocalculation of ideal strength and phonon instability of graphene under tension. Phys Rev B 2007;76.
[17] Politano A, Marino AR, Campi D, Farías D, Miranda R, Chiarello G. Elastic properties of a macroscopic graphene sample from phonon dispersion measurements. Carbon 2012;50:4903–10.
[18] Koenig SP, Boddeti NG, Dunn ML, Bunch JS. Ultrastrong adhesion of graphene membranes. Nat Nanotechnol 2011;6:543–6.
[19] Lier GV, Alsenoy CV, Doren VV, Geerlings P. Ab initio study of the elastic properties of single-walled carbon nanotubes and graphene. Chem Phys Lett 2000;326:181–5.
[20] Li C, Chou T-W. A structural mechanics approach for the analysis of carbon nanotubes. Int J Solids Struct 2003;40:2487–99.
[21] Shokrieh MM, Rafiee R. Prediction of Young's modulus of graphene sheets and carbon nanotubes using nanoscale continuum mechanics approach. Mater Des 2010;31:790–5.
[22] Kvashnin DG, Sorokin PB. Effect of ultrahigh stiffness of defective graphene from atomistic point of view. J Phys Chem Lett 2015;6:2384–7.
[23] Potts JR, Dreyer DR, Bielawski CW, Ruoff RS. Graphene-based polymer nanocomposites. Polymer 2011;52:5–25.
[24] Kuilla T, Bhadra S, Yao D, Kim NH, Bose S, Lee JH. Recent advances in graphene based polymer composites. Prog Polym Sci 2010;35:1350–75.
[25] Singh V, Joung D, Zhai L, Das S, Khondaker SI, Seal S. Graphene based materials: Past, present and future. Prog Mater Sci 2011;56:1178–271.
[26] Huang X, Qi X, Boey F, Zhang H. Graphene-based composites. Chem Soc Rev 2012;41:666–86.
[27] Papageorgiou DG, Kinloch IA, Young RJ. Mechanical properties of graphene and graphene-based nanocomposites. Prog Mater Sci 2017;90:75–127.
[28] Tjong SC. Recent progress in the development and properties of novel metal matrix nanocomposites reinforced with carbon nanotubes and graphene nanosheets. Mater Sci Eng: R: Rep 2013;74:281–350.
[29] Hu Z, Tong G, Lin D, Chen C, Guo H, Xu J, et al. Graphene-reinforced metal matrix nanocomposites – a review. Mater Sci Technol 2016;32:930–53.
[30] Nieto A, Bisht A, Lahiri D, Zhang C, Agarwal A. Graphene reinforced metal and ceramic matrix composites: a review. Int Mater Rev 2016;62:241–302.
[31] Kalaitzidou K, Fukushima H, Drzal LT. A new compounding method for exfoliated graphite–polypropylene nanocomposites with enhanced flexural properties and lower percolation threshold. Compos Sci Technol 2007;67:2045–51.
[32] Kalaitzidou K, Fukushima H, Drzal LT. Mechanical properties and morphological characterization of exfoliated graphite–polypropylene nanocomposites. Compos A Appl Sci Manuf 2007;38:1675–82.
[33] Ramanathan T, Abdala AA, Stankovich S, Dikin DA, Herrera-Alonso M, Piner RD, et al. Functionalized graphene sheets for polymer nanocomposites. Nat Nanotechnol 2008;3:327–31.
[34] Liang J, Huang Y, Zhang L, Wang Y, Ma Y, Guo T, et al. Molecular-Level Dispersion of Graphene into Poly(vinyl alcohol) and Effective Reinforcement of their Nanocomposites. Adv Funct Mater 2009;19:2297–302.
[35] Rafiee MA, Rafiee J, Wang Z, Song H, Yu Z-Z, Koratkar N. Enhanced mechanical properties of nanocomposites at low graphene content. ACS Nano 2009;3:3884–90.
[36] Song P, Cao Z, Cai Y, Zhao L, Fang Z, Fu S. Fabrication of exfoliated graphene-based polypropylene nanocomposites with enhanced mechanical and thermal properties. Polymer 2011;52:4001–10.
[37] Naebe M, Wang J, Amini A, Khayyam H, Hameed N, Li LH, et al. Mechanical property and structure of covalent functionalised graphene/epoxy nanocomposites. Sci Rep 2014;4:4375.
[38] Pathak AK, Borah M, Gupta A, Yokozeki T, Dhakate SR. Improved mechanical properties of carbon fiber/graphene oxide-epoxy hybrid composites. Compos Sci Technol 2016;135:28–38.
[39] Wang X, Liu X, Yuan H, Liu H, Liu C, Li T, et al. Non-covalently functionalized graphene strengthened poly(vinyl alcohol). Mater Des 2018;139:372–9.
[40] Wang J, Li Z, Fan G, Pan H, Chen Z, Zhang D. Reinforcement with graphene nanosheets in aluminum matrix composites. Scr Mater 2012;66:594–7.
[41] Hwang J, Yoon T, Jin SH, Lee J, Kim TS, Hong SH, et al. Enhanced mechanical properties of graphene/copper nanocomposites using a molecular-level mixing process. Adv Mater. 2013;25:6724–9.
[42] Li Z, Guo Q, Li Z, Fan G, Xiong DB, Su Y, et al. Enhanced mechanical properties of graphene (reduced graphene oxide)/aluminum composites with a bioinspired nanolaminated structure. Nano Lett 2015;15:8077–83.
[43] Yolshina LA, Muradymov RV, Korsun IV, Yakovlev GA, Smirnov SV. Novel aluminum-graphene and aluminum-graphite metallic composite materials: Synthesis and properties. J Alloy Compd 2016;663:449–59.
[44] Zhang D, Zhan Z. Preparation of graphene nanoplatelets-copper composites by a modified semi-powder method and their mechanical properties. J Alloy Compd 2016;658:663–71.
[45] Cao M, Xiong D-B, Tan Z, Ji G, Amin-Ahmadi B, Guo Q, et al. Aligning graphene in bulk copper: Nacre-inspired nanolaminated architecture coupled with in-situ processing for enhanced mechanical properties and high electrical conductivity. Carbon 2017;117:65–74.
[46] Jiang J, He X, Du J, Pang X, Yang H, Wei Z. In-situ fabrication of graphene-nickel matrix composites. Mater Lett 2018;220:178–81.
[47] Yuan Q-h, Zhou G-h, Liao L, Liu Y, Luo L. Interfacial structure in AZ91 alloy composites reinforced by graphene nanosheets. Carbon 2018;127:177–86.
[48] Bever MB, Duwez PE. Gradients in composite materials. Mater Sci Eng 1972;10:1–8.
[49] Shen M, Bever MB. Gradients in polymeric materials. J Mater Sci 1972;7:741–6.
[50] Niino M, Maeda S. Recent development status of functionally gradient materials. ISIJ Int 1990;30:699–703.
[51] Koizumi M. FGM activities in Japan. Compos B Eng 1997;28:1–4.
[52] Piggott M. Load bearing fibre composites. New York, Boston, Dordrecht, London, Moscow: Kluwer Academic Publisher; 2002.
[53] Jones RM. Mechanics of composite materials. Taylor & Francis; 1999.
[54] Cox HL. The elasticity and strength of paper and other fibrous materials. Br J Appl Phys 1952;3:72.
[55] Halpin JC. Stiffness and expansion estimates for oriented short fiber composites. J Compos Mater 1969;3:732–4.
[56] Halpin JC, Kardos JL. The Halpin-Tsai equations: a review. Polym Eng Sci 1976;16:344–52.
[57] Eshelby JD. The determination of the elastic field of an ellipsoidal inclusion, and related problems. Proc Roy Soc London 1957;241:376–96.
[58] Mori T, Tanaka K. Average stress in matrix and average elastic energy of materials with misfitting inclusions. Acta Metall 1973;21:571–4.
[59] Hill R. A self-consistent mechanics of composite materials. J Mech Phys Solids 1965;13:213–22.
[60] Hashin Z, Shtrikman S. A variational approach to the theory of the elastic behaviour of polycrystals. J Mech Phys Solids 1962;10:343–52.
[61] Hashin Z, Shtrikman S. On some variational principles in anisotropic and nonhomogeneous elasticity. J Mech Phys Solids 1962;10:335–42.
[62] Schapery RA. Thermal expansion coefficients of composite materials based on energy principles. J Compos Mater 1968;2:380–404.
[63] Zheng QS, Du DX. An explicit and universally applicable estimate for the effective properties of multiphase composites which accounts for inclusion distribution. J Mech Phys Solids 2001;49:2765–88.
[64] Chu K, Jia C-c. Li W-s. Effective thermal conductivity of graphene-based composites. Appl Phys Lett 2012;101:121916.
[65] Landau LD, Lifshitz EM, Pitaevskii LP. Electrodynamics of Continuous Media. New York: Pergamon Press; 1984.
[66] Taya M. Electronic composites: modeling, characterization, processing, and MEMS applications. Cambridge University Press; 2005.
[67] Facca AG, Kortschot MT, Yan N. Predicting the elastic modulus of natural fibre reinforced thermoplastics. Compos A Appl Sci Manuf 2006;37:1660–71.
[68] Krenchel H. Fibre reinforcement: theoretical and practical investigations of the elasticity and strength of fibre-reinforced materials: Akademisk forlag; 1964.
[69] Sun R, Li L, Zhao S, Feng C, Kitipornchai S, Yang J. Temperature-dependent mechanical properties of defective graphene reinforced polymer nanocomposite. Mech Adv Mater Struct 2019;1–10.
[70] Lin F, Xiang Y, Shen H-S. Temperature dependent mechanical properties of graphene reinforced polymer nanocomposites – A molecular dynamics simulation. Compos B Eng 2017;111:261–9.
[71] Sun R, Li L, Feng C, Kitipornchai S, Yang J. Tensile behavior of polymer nanocomposite reinforced with graphene containing defects. Eur Polym J 2018;98:475–82.
[72] Sun R, Li L, Feng C, Kitipornchai S, Yang J. Tensile property enhancement of defective graphene/epoxy nanocomposite by hydrogen functionalization. Compos Struct 2019;224.
[73] Shen H-S, Lin F, Xiang Y. Nonlinear bending and thermal postbuckling of functionally graded graphene-reinforced composite laminated beams resting on elastic foundations. Eng Struct 2017;140:89–97.
[74] Shen H-S, Xiang Y, Lin F. Nonlinear vibration of functionally graded graphene-reinforced composite laminated plates in thermal environments. Comput Methods Appl Mech Eng 2017;319:175–93.
[75] Shen H-S, Xiang Y, Lin F. Nonlinear bending of functionally graded graphene-reinforced composite laminated plates resting on elastic foundations in thermal environments. Compos Struct 2017;170:80–90.
[76] Shen H-S, Xiang Y, Lin F, Hui D. Buckling and postbuckling of functionally graded graphene-reinforced composite laminated plates in thermal environments. Compos B Eng 2017;119:67–78.
[77] Shen H-S, Lin F, Xiang Y. Nonlinear vibration of functionally graded graphene-reinforced composite laminated beams resting on elastic foundations in thermal environments. Nonlinear Dyn 2017;90:899–914.
[78] Benveniste Y. A new approach to the application of Mori-Tanaka's theory in composite materials. Mech Mater 1987;6:147–57.
[79] Tandon GP, Weng GJ. The effect of aspect ratio of inclusions on the elastic properties of unidirectionally aligned composites. Polym Compos 1984;5:327–33.
[80] Shen H-S, Xiang Y. Postbuckling behavior of functionally graded graphene-reinforced composite laminated cylindrical shells under axial compression in thermal environments. Comput Methods Appl Mech Eng 2018;330:64–82.
[81] Turner PS. The problem of thermal-expansion stresses in reinforced plastics. J Res Nat Bur Stand 1946;37:239–50.
[82] Kerner EH. The elastic and thermo-elastic properties of composite media. Proc Phys Soc Section B 1956;69:808–13.
[83] Rosen BW, Hashin Z. Effective thermal expansion coefficients and specific heats of composite materials. Int J Eng Sci 1970;8:157–73.
[84] Yang B, Kitipornchai S, Yang Y-F, Yang J. 3D thermo-mechanical bending solution of functionally graded graphene reinforced circular and annular plates. Appl Math Model 2017;49:69–86.
[85] Yang B, Yang J, Kitipornchai S. Thermoelastic analysis of functionally graded graphene reinforced rectangular plates based on 3D elasticity. Meccanica

2017;52:2275–92.
[86] Yang B, Mei J, Chen D, Yu F, Yang J. 3D thermo-mechanical solution of transversely isotropic and functionally graded graphene reinforced elliptical plates. Compos Struct 2018;184:1040–8.
[87] Wang Y, Feng C, Wang X, Zhao Z, Romero CS, Dong Y, et al. Nonlinear static and dynamic responses of graphene platelets reinforced composite beam with dielectric permittivity. Appl Math Model 2019;71:298–315.
[88] Wang Y, Feng C, Santiuste C, Zhao Z, Yang J. Buckling and postbuckling of dielectric composite beam reinforced with Graphene Platelets (GPLs). Aerosp Sci Technol 2019;91:208–18.
[89] Wang Y, Feng C, Wang X, Zhao Z, Romero CS, Yang J. Nonlinear free vibration of graphene platelets (GPLs)/polymer dielectric beam. Smart Mater Struct 2019;28:055013.
[90] Zhou Z, Ni Y, Tong Z, Zhu S, Sun J, Xu X. Accurate nonlinear stability analysis of functionally graded multilayer hybrid composite cylindrical shells subjected to combined loads. Mater Des 2019;182:108035.
[91] Arefi M, Mohammad-Rezaei Bidgoli E, Dimitri R, Bacciocchi M, Tornabene F. Nonlocal bending analysis of curved nanobeams reinforced by graphene nanoplatelets. Compos B Eng 2019;166:1–12.
[92] Polit O, Anant C, Anirudh B, Ganapathi M. Functionally graded graphene reinforced porous nanocomposite curved beams: Bending and elastic stability using a higher-order model with thickness stretch effect. Compos B Eng 2019;166:310–27.
[93] Anirudh B, Ganapathi M, Anant C, Polit O. A comprehensive analysis of porous graphene-reinforced curved beams by finite element approach using higher-order structural theory: Bending, vibration and buckling. Compos Struct 2019;222:110899.
[94] Song M, Yang J, Kitipornchai S. Bending and buckling analyses of functionally graded polymer composite plates reinforced with graphene nanoplatelets. Compos B Eng 2018;134:106–13.
[95] Li K, Wu D, Chen X, Cheng J, Liu Z, Gao W. Isogeometric Analysis of functionally graded porous plates reinforced by graphene platelets. Compos Struct 2018;204:114–30.
[96] Zhao Z, Feng C, Wang Y, Yang J. Bending and vibration analysis of functionally graded trapezoidal nanocomposite plates reinforced with graphene nanoplatelets (GPLs). Compos Struct 2017;180:799–808.
[97] García-Macías E, Rodríguez-Tembleque L, Sáez A. Bending and free vibration analysis of functionally graded graphene vs. carbon nanotube reinforced composite plates. Compos Struct 2018;186:123–38.
[98] Sahmani S, Aghdam MM, Rabczuk T. Nonlinear bending of functionally graded porous micro/nano-beams reinforced with graphene platelets based upon nonlocal strain gradient theory. Compos Struct 2018;186:68–78.
[99] Rafiee M, Nitzsche F, Labrosse MR. Modeling and mechanical analysis of multiscale fiber-reinforced graphene composites: Nonlinear bending, thermal postbuckling and large amplitude vibration. Int J Non Linear Mech 2018;103:104–12.
[100] Liu Z, Yang C, Gao W, Wu D, Li G. Nonlinear behaviour and stability of functionally graded porous arches with graphene platelets reinforcements. Int J Eng Sci 2019;137:37–56.
[101] Zhao Z, Feng C, Dong Y, Wang Y, Yang J. Geometrically nonlinear bending of functionally graded nanocomposite trapezoidal plates reinforced with graphene platelets (GPLs). Int J Mech Mater Des 2019;15:791–800.
[102] Gholami R, Ansari R. Large deflection geometrically nonlinear analysis of functionally graded multilayer graphene platelet-reinforced polymer composite rectangular plates. Compos Struct 2017;180:760–71.
[103] Guo H, Cao S, Yang T, Chen Y. Geometrically nonlinear analysis of laminated composite quadrilateral plates reinforced with graphene nanoplatelets using the element-free IMLS-Ritz method. Compos B Eng 2018;154:216–24.
[104] Shen H-S, Xiang Y, Fan Y, Hui D. Nonlinear bending analysis of FG-GRC laminated cylindrical panels on elastic foundations in thermal environments. Compos B Eng 2018;141:148–57.
[105] Kitipornchai S, Chen D, Yang J. Free vibration and elastic buckling of functionally graded porous beams reinforced by graphene platelets. Mater Des 2017;116:656–65.
[106] Jiao P, Alavi AH. Buckling analysis of graphene-reinforced mechanical metamaterial beams with periodic webbing patterns. Int J Eng Sci 2018;131:1–18.
[107] Tam M, Yang Z, Zhao S, Yang J. Vibration and buckling characteristics of functionally graded graphene nanoplatelets reinforced composite beams with open edge cracks. Materials. 2019;12:1412.
[108] Song M, Gong Y, Yang J, Zhu W, Kitipornchai S. Free vibration and buckling analyses of edge-cracked functionally graded multilayer graphene nanoplatelet-reinforced composite beams resting on an elastic foundation. J Sound Vib 2019;458:89–108.
[109] Yang J, Chen D, Kitipornchai S. Buckling and free vibration analyses of functionally graded graphene reinforced porous nanocomposite plates based on Chebyshev-Ritz method. Compos Struct 2018;193:281–94.
[110] Mirzaei M, Kiani Y. Isogeometric thermal buckling analysis of temperature dependent FG graphene reinforced laminated plates using NURBS formulation. Compos Struct 2017;180:606–16.
[111] Lei Z, Su Q, Zeng H, Zhang Y, Yu C. Parametric studies on buckling behavior of functionally graded graphene-reinforced composites laminated plates in thermal environment. Compos Struct 2018;202:695–709.
[112] Wang Y, Feng C, Zhao Z, Lu F, Yang J. Torsional buckling of graphene platelets (GPLs) reinforced functionally graded cylindrical shell with cutout. Compos Struct 2018;197:72–9.
[113] Wang Y, Feng C, Zhao Z, Yang J. Buckling of graphene platelet reinforced composite cylindrical shell with cutout. Int J Struct Stab Dyn 2018;18:1850040.
[114] Wang Y, Feng C, Zhao Z, Yang J. Eigenvalue buckling of functionally graded cylindrical shells reinforced with graphene platelets (GPL). Compos Struct 2018;202:38–46.
[115] Liu D, Kitipornchai S, Chen W, Yang J. Three-dimensional buckling and free vibration analyses of initially stressed functionally graded graphene reinforced composite cylindrical shell. Compos Struct 2018;189:560–9.
[116] Barati MR, Zenkour AM. Post-buckling analysis of refined shear deformable graphene platelet reinforced beams with porosities and geometrical imperfection. Compos Struct 2017;181:194–202.
[117] Kiani Y, Mirzaei M. Enhancement of non-linear thermal stability of temperature dependent laminated beams with graphene reinforcements. Compos Struct 2018;186:114–22.
[118] Song M, Chen L, Yang J, Zhu W, Kitipornchai S. Thermal buckling and post-buckling of edge-cracked functionally graded multilayer graphene nanocomposite beams on an elastic foundation. Int J Mech Sci 2019;161–162:105040.
[119] Yang Z, Yang J, Liu A, Fu J. Nonlinear in-plane instability of functionally graded multilayer graphene reinforced composite shallow arches. Compos Struct 2018;204:301–12.
[120] Huang Y, Yang Z, Liu A, Fu J. Nonlinear buckling analysis of functionally graded graphene reinforced composite shallow arches with elastic rotational constraints under uniform radial load. Materials 2018;11:910.
[121] Yang Z, Huang Y, Liu A, Fu J, Wu D. Nonlinear in-plane buckling of fixed shallow functionally graded graphene reinforced composite arches subjected to mechanical and thermal loading. Appl Math Model 2019;70:315–27.
[122] Song M, Yang J, Kitipornchai S, Zhu W. Buckling and postbuckling of biaxially compressed functionally graded multilayer graphene nanoplatelet-reinforced polymer composite plates. Int J Mech Sci 2017;131–132:345–55.
[123] Yang J, Dong J, Kitipornchai S. Unilateral and bilateral buckling of functionally graded corrugated thin plates reinforced with graphene nanoplatelets. Compos Struct 2019;209:789–801.
[124] Wu H, Kitipornchai S, Yang J. Thermal buckling and postbuckling of functionally graded graphene nanocomposite plates. Mater Des 2017;132:430–41.
[125] Yu Y, Shen H-S, Wang H, Hui D. Postbuckling of sandwich plates with graphene-reinforced composite face sheets in thermal environments. Compos B Eng 2018;135:72–83.
[126] Shen H-S, Xiang Y, Lin F. Thermal buckling and postbuckling of functionally graded graphene-reinforced composite laminated plates resting on elastic foundations. Thin-Walled Struct 2017;118:229–37.
[127] Shen H-S, Xiang Y, Fan Y. Postbuckling of functionally graded graphene-reinforced composite laminated cylindrical panels under axial compression in thermal environments. Int J Mech Sci 2018;135:398–409.
[128] Kiani Y. NURBS-based isogeometric thermal postbuckling analysis of temperature dependent graphene reinforced composite laminated plates. Thin-Walled Struct 2018;125:211–9.
[129] Li Z, Zheng J. Analytical consideration and numerical verification of the confined functionally graded porous ring with graphene platelet reinforcement. Int J Mech Sci 2019;161–162:105079.
[130] Dong YH, He LW, Wang L, Li YH, Yang J. Buckling of spinning functionally graded graphene reinforced porous nanocomposite cylindrical shells: An analytical study. Aerosp Sci Technol 2018;82–83:466–78.
[131] Zhou Z, Ni Y, Tong Z, Zhu S, Sun J, Xu X. Accurate nonlinear buckling analysis of functionally graded porous graphene platelet reinforced composite cylindrical shells. Int J Mech Sci 2019;151:537–50.
[132] Sun J, Ni Y, Gao H, Zhu S, Tong Z, Zhou Z. Torsional buckling of functionally graded multilayer graphene nanoplatelet-reinforced cylindrical shells. Int J Struct Stab Dyn 2019.
[133] Sahmani S, Aghdam MM. A nonlocal strain gradient hyperbolic shear deformable shell model for radial postbuckling analysis of functionally graded multilayer GPLRC nanoshells. Compos Struct 2017;178:97–109.
[134] Sahmani S, Aghdam MM. Nonlinear instability of axially loaded functionally graded multilayer graphene platelet-reinforced nanoshells based on nonlocal strain gradient elasticity theory. Int J Mech Sci 2017;131–132:95–106.
[135] Shen H-S, Xiang Y. Postbuckling of functionally graded graphene-reinforced composite laminated cylindrical shells subjected to external pressure in thermal environments. Thin-Walled Struct 2018;124:151–60.
[136] Muni Rami Reddy R, Karunasena W, Lokuge W. Free vibration of functionally graded-GPL reinforced composite plates with different boundary conditions. Aerosp Sci Technol 2018;78:147–56.
[137] Thai CH, Ferreira AJM, Tran TD, Phung-Van P. Free vibration, buckling and bending analyses of multilayer functionally graded graphene nanoplatelets reinforced composite plates using the NURBS formulation. Compos Struct 2019;220:749–59.
[138] Guo H, Cao S, Yang T, Chen Y. Vibration of laminated composite quadrilateral plates reinforced with graphene nanoplatelets using the element-free IMLS-Ritz method. Int J Mech Sci 2018;142–143:610–21.
[139] Malekzadeh P, Setoodeh AR, Shojaee M. Vibration of FG-GPLs eccentric annular plates embedded in piezoelectric layers using a transformed differential quadrature method. Comput Methods Appl Mech Eng 2018;340:451–79.
[140] Arefi M, Mohammad-Rezaei Bidgoli E, Dimitri R, Tornabene F. Free vibrations of functionally graded polymer composite nanoplates reinforced with graphene nanoplatelets. Aerosp Sci Technol 2018;81:108–17.
[141] Niu Y, Zhang W, Guo XY. Free vibration of rotating pretwisted functionally graded composite cylindrical panel reinforced with graphene platelets. Eur J Mech A Solids 2019;77:103798.
[142] Dong YH, Li YH, Chen D, Yang J. Vibration characteristics of functionally graded graphene reinforced porous nanocomposite cylindrical shells with spinning motion. Compos B Eng 2018;145:1–13.

[143] Wang YQ, Liu YF, Zu JW. Size-dependent vibration of circular cylindrical polymeric microshells reinforced with graphene platelets. Int J Appl Mech 2019;11:1950036.
[144] Wang A, Chen H, Hao Y, Zhang W. Vibration and bending behavior of functionally graded nanocomposite doubly-curved shallow shells reinforced by graphene nanoplatelets. Results Phys 2018;9:550–9.
[145] Moradi-Dastjerdi R, Behdinan K. Thermoelastic static and vibrational behaviors of nanocomposite thick cylinders reinforced with graphene. Steel Compos Struct 2019;31:529–39.
[146] Feng C, Kitipornchai S, Yang J. Nonlinear free vibration of functionally graded polymer composite beams reinforced with graphene nanoplatelets (GPLs). Eng Struct 2017;140:110–9.
[147] Chen D, Yang J, Kitipornchai S. Nonlinear vibration and postbuckling of functionally graded graphene reinforced porous nanocomposite beams. Compos Sci Technol 2017;142:235–45.
[148] Gao K, Gao W, Chen D, Yang J. Nonlinear free vibration of functionally graded graphene platelets reinforced porous nanocomposite plates resting on elastic foundation. Compos Struct 2018;204:831–46.
[149] Shen H-S, Xiang Y, Fan Y, Hui D. Nonlinear vibration of functionally graded graphene-reinforced composite laminated cylindrical panels resting on elastic foundations in thermal environments. Compos B Eng 2018;136:177–86.
[150] Kiani Y. Isogeometric large amplitude free vibration of graphene reinforced laminated plates in thermal environment using NURBS formulation. Comput Methods Appl Mech Eng 2018;332:86–101.
[151] Mao J-J, Zhang W. Linear and nonlinear free and forced vibrations of graphene reinforced piezoelectric composite plate under external voltage excitation. Compos Struct 2018;203:551–65.
[152] Dong YH, Zhu B, Wang Y, Li YH, Yang J. Nonlinear free vibration of graded graphene reinforced cylindrical shells: Effects of spinning motion and axial load. J Sound Vib 2018;437:79–96.
[153] Wang YQ, Ye C, Zu JW. Nonlinear vibration of metal foam cylindrical shells reinforced with graphene platelets. Aerosp Sci Technol 2019;85:359–70.
[154] Shen H-S, Xiang Y, Fan Y. Nonlinear vibration of functionally graded graphene-reinforced composite laminated cylindrical shells in thermal environments. Compos Struct 2017;182:447–56.
[155] Wu H, Yang J, Kitipornchai S. Dynamic instability of functionally graded multilayer graphene nanocomposite beams in thermal environment. Compos Struct 2017;162:244–54.
[156] Zhao S, Yang Z, Kitipornchai S, Yang J. Dynamic instability of functionally graded porous arches reinforced by graphene platelets. Thin-Walled Struct 2020;147:106491.
[157] Yang Z, Liu A, Yang J, Fu J, Yang B. Dynamic buckling of functionally graded graphene nanoplatelets reinforced composite shallow arches under a step central point load. J Sound Vib 2020;465:115019.
[158] Wu H, Yang J, Kitipornchai S. Parametric instability of thermo-mechanically loaded functionally graded graphene reinforced nanocomposite plates. Int J Mech Sci 2018;135:431–40.
[159] Shen H-S, Xiang Y, Fan Y. A novel technique for nonlinear dynamic instability analysis of FG-GRC laminated plates. Thin-Walled Struct 2019;139:389–97.
[160] Li X, Song M, Yang J, Kitipornchai S. Primary and secondary resonances of functionally graded graphene platelet-reinforced nanocomposite beams. Nonlinear Dyn 2018;95:1807–26.
[161] Karami B, Shahsavari D, Janghorban M, Tounsi A. Resonance behavior of functionally graded polymer composite nanoplates reinforced with graphene nanoplatelets. Int J Mech Sci 2019;156:94–105.
[162] Gholami R, Ansari R. Nonlinear harmonically excited vibration of third-order shear deformable functionally graded graphene platelet-reinforced composite rectangular plates. Eng Struct 2018;156:197–209.
[163] Dong Y, Li X, Gao K, Li Y, Yang J. Harmonic resonances of graphene-reinforced nonlinear cylindrical shells: effects of spinning motion and thermal environment. Nonlinear Dyn 2019.
[164] Wang Y, Xie K, Fu T, Shi C. Vibration response of a functionally graded graphene nanoplatelet reinforced composite beam under two successive moving masses. Compos Struct 2019;209:928–39.
[165] Nguyen LB, Nguyen NV, Thai CH, Ferreira AMJ, Nguyen-Xuan H. An isogeometric Bézier finite element analysis for piezoelectric FG porous plates reinforced by graphene platelets. Compos Struct 2019;214:227–45.
[166] Li Q, Wu D, Chen X, Liu L, Yu Y, Gao W. Nonlinear vibration and dynamic buckling analyses of sandwich functionally graded porous plate with graphene platelet reinforcement resting on Winkler-Pasternak elastic foundation. Int J Mech Sci 2018;148:596–610.
[167] Xu Z, Huang Q. Vibro-acoustic analysis of functionally graded graphene-reinforced nanocomposite laminated plates under thermal-mechanical loads. Eng Struct 2019;186:345–55.
[168] Wang A, Chen H, Zhang W. Nonlinear transient response of doubly curved shallow shells reinforced with graphene nanoplatelets subjected to blast loads considering thermal effects. Compos Struct 2019;225:111063.
[169] Fan Y, Xiang Y, Shen H-S, Wang H. Low-velocity impact response of FG-GRC laminated beams resting on visco-elastic foundations. Int J Mech Sci 2018;141:117–26.
[170] Fan Y, Xiang Y, Shen H-S, Hui D. Nonlinear low-velocity impact response of FG-GRC laminated plates resting on visco-elastic foundations. Compos B Eng 2018;144:184–94.
[171] Song M, Li X, Kitipornchai S, Bi Q, Yang J. Low-velocity impact response of geometrically nonlinear functionally graded graphene platelet-reinforced nanocomposite plates. Nonlinear Dyn 2018;95:2333–52.
[172] Dong YH, Zhu B, Wang Y, He LW, Li YH, Yang J. Analytical prediction of the impact response of graphene reinforced spinning cylindrical shells under axial and thermal loads. Appl Math Model 2019;71:331–48.
[173] Li Z, Zheng J, Chen Y, Sun Q, Zhang Z. Effect of temperature variations on the stability mechanism of the confined functionally graded porous arch with nanocomposites reinforcement under mechanical loading. Compos B Eng 2019;176:107330.
[174] Sobhy M, Alakel Abazid M. Dynamic and instability analyses of FG graphene-reinforced sandwich deep curved nanobeams with viscoelastic core under magnetic field effect. Compos B Eng 2019;174:106966.
[175] Sahmani S, Aghdam MM. Nonlocal strain gradient beam model for nonlinear vibration of prebuckled and postbuckled multilayer functionally graded GPLRC nanobeams. Compos Struct 2017;179:77–88.
[176] Sahmani S, Aghdam MM, Rabczuk T. Nonlocal strain gradient plate model for nonlinear large-amplitude vibrations of functionally graded porous micro/nanoplates reinforced with GPLs. Compos Struct 2018;198:51–62.
[177] Narayan DA, Zineb TB, Polit O, Pradyumna B, Ganapathi M. Large amplitude free flexural vibrations of functionally graded graphene platelets reinforced porous composite curved beams using finite element based on trigonometric shear deformation theory. Int J Non Linear Mech 2019;116:302–17.
[178] Kiani Y. Buckling of functionally graded graphene reinforced conical shells under external pressure in thermal environment. Compos B Eng 2019;156:128–37.
[179] Fan Y, Xiang Y, Shen H-S. Nonlinear forced vibration of FG-GRC laminated plates resting on visco-Pasternak foundations. Compos Struct 2019;209:443–52.
[180] Guo X, Jiang P, Zhang W, Yang J, Kitipornchai S, Sun L. Nonlinear dynamic analysis of composite piezoelectric plates with graphene skin. Compos Struct 2018;206:839–52.
[181] Mirjavadi SS, Forsat M, Hamouda AMS, Barati MR. Dynamic response of functionally graded graphene nanoplatelet reinforced shells with porosity distributions under transverse dynamic loads. Mater Res Express 2019;6:075045.